ADVANCED ENERGY MATERIALS
www.advenergymat.de

Stability of Organic Solar Cells: The Influence of Nanostructured Carbon Materials

*Isabel Fraga Domínguez, Andreas Distler, and Larry Lüer**

Organic solar cells (OSCs) are lightweight, have adaptable colors, and can be produced in low-cost procedures on transparent and flexible surfaces. This makes them attractive for markets in which other technologies cannot compete, for example in architectural and consumer product integration. However, both efficiencies and long term operational stability of OSCs do not yet meet the standards set by their inorganic counterparts. This review compiles the growing knowledge about how nanostructured carbon materials, such as fullerenes and carbon nanotubes, decisively influence the operational stability of organic photovoltaics. Firstly, important degradation pathways are introduced and a differential detection scheme is set up to find the dominant loss channel by means of state-of-the-art characterization methods. Then, fullerenes ability to both stabilize and destabilize the donor polymer against photooxidation via different mechanisms (e.g., inner filter effect or radical scavenging) is examined in detail. The "burn-in" problem, an initial rapid efficiency loss in $PC_{60}BM$-based OSCs, is shown to derive from light-induced $PC_{60}BM$ dimerization, an effect that can also be positively exploited to reduce thermal degradation. Finally, thermal stabilization via additional approaches involving the fullerene derivative, such as crosslinking or incorporation into block copolymers, is presented.

1. Introduction

Organic solar cells (OSCs), in which the photoactive layer is composed of compounds from organic synthesis, are an interesting alternative to classical inorganic solar cells especially for targeted individual solutions close to the customer. OSCs can be processed from solution in a roll-to-roll procedure, yielding transparent films with optical quality apt for the applications on windows, produced at very low energy impact as compared to inorganic solar cells. The skills of organic chemists allow the production of solar cells with colors adapted for the target application, e.g., absorbing in the near infrared (NIR) but transmitting visible light for office buildings, or a wavelength selective transmission spectrum adapted to the action spectrum of plants in greenhouses.[1] Broad angular acceptance, positive thermal coefficients and low light increases of the power conversion efficiency (PCE) favor the application of OSCs especially under non-optimum conditions close to the customer, such as in densely populated areas or in indoor applications for low power devices such as wireless transmitters and sensors. From an environmental perspective, all the aforementioned applications are especially encouraging because they are not in competition with other area uses for example in food production; from a commercial perspective their operation is low cost because the infrastructure (support, grid, theft protection, operating personnel, etc.) is in place anyway for the objects in which OSCs are integrated.

Maximum certified PCE values reported for OSCs are above 13%,[2] while the currently achievable module performances are still significantly lower than the efficiencies reached by the market dominating inorganic technologies. However, looking more closely at the reasons for the PCE limitations in OSCs, we find that often these limitations are by no means detrimental for certain markets. For example, an incomplete absorption yield in the visible spectral region certainly reduces PCE but makes the solar module colored and transparent, which is a unique feature of organic photovoltaics for certain applications, e.g., in architecture. As another example, low fill factors, a typical problem of the organic phase with its low charge mobility limiting the overall device performance, actually improve under low-light application, e.g., indoor, where other photovoltaic technologies exhibit severe losses in fill factor and PCE.[3]

The main Achilles heel of OSCs is their limited operational stability.[4] The potential degradation routes of organic photovoltaics are manifold and some even derive directly from their working principle. For example, the π-conjugated compounds used as active materials, namely a polymer donor and a fullerene acceptor, are forming a so-called bulk heterojunction, an arrangement of domains that is determined by the best compromise of electronic, optical, and transport properties.[5] This arrangement is, however, generally not the thermodynamic equilibrium. Therefore, the nanoscale morphologies in the active layer tend to change during operation. Below, we show in detail the consequences of morphological changes on the electrical performance of OSCs, and we report on attempts to stabilize the active layer morphology.

Another degradation route addresses carbon-carbon double bonds, which are inevitably needed for π conjugation but represent a reactive species. Woodward – Hoffman rules predict a

Dr. I. Fraga Domínguez, Dr. A. Distler
Belectric OPV GmbH
Landgrabenstr. 94, 90443 Nürnberg, Germany
Dr. L. Lüer
IMDEA Nanociencia
C/ Faraday, 9, 28049 Madrid, Spain
E-mail: larry.luer@imdea.org

DOI: 10.1002/aenm.201601320

photochemical pathway for a 2+2 cycloaddition of two double bonds from adjacent conjugated systems. Below, we show that this mechanism is indeed observed in OSCs, causing dimerization of fullerene derivatives often used as acceptor materials.[6] We discuss the most plausible model for the dimerization, evaluate the consequences for OSCs electrical performance, and show how it can be avoided.

Finally, the reaction of molecular oxygen with a π-conjugated system leads to the formation of carbonyl bonds.[7] As this reaction is exothermic, it cannot be avoided, leading eventually to irreversible degradation of the conjugation with negative consequences on light harvesting and charge transport. Intense efforts are therefore directed towards reducing the reaction rate as much as possible.[8] On the one hand, knowledge of the precise degradation mechanism is essential.[7e] As we show below, a radical pathway has been found to be dominant for the photooxidation of many donor polymers.[7d,e,9] Consequently, optimizing the radical scavenging properties of fullerene acceptors presents a decisive handle towards OSCs stabilization. On the other hand, the concentration of molecular oxygen can be kept on negligible levels by appropriate encapsulation.[10] Cost arguments however pose a limit to the employment of ultrahigh barrier foils. While small area organic light emitting diode (OLED) displays usually operate under low-light conditions and can be well protected by encapsulation, this approach is inhibitive for large area OSCs panels exposed to "1 sun". Thus, we describe efforts to make OSCs active layers intrinsically more stable against photooxidation, which allows the use of competitively priced encapsulation while still reaching a sufficient lifetime.

This paper is organized as follows. In section 2, the elementary degradation processes that cause electrical performance loss in organic solar cells are introduced. It is distinguished between charge generation losses and charge extraction losses, because these are quantities that can be monitored by routine measurements in a non-destructive way, thus allowing for an efficient feedback between characterization and device technology. Special emphasis is given to the influence of the morphology on the electrical parameters. In section 3, we describe the degradation of the active layer. We distinguish between morphological degradation and photochemical degradation. In the case of photooxidation, both reversible and irreversible contributions are discussed. In section 4, the influence of carbon materials on the degradation of the active layers in OSCs is examined. We show that fullerenes decisively influence the rate of photooxidation of the donor polymers and evaluate the steric and electronic contribution to this effect. Dimerization of fullerenes is found to contribute to the burn-in phenomenon often found in OSCs. Finally, in section 5 we conclude the state of the art and outline promising current and future research directions.

Isabel Fraga Domínguez obtained her PhD from the Université Blaise Pascal (Clermont-Ferrand) and Aston University (Birmingham) in 2015, under the supervision of Dr. Agnès Rivaton, Dr. Pierre-Olivier Bussière and Dr. Paul D Topham. Her PhD dissertation focused on the identification of degradation mechanisms in organic solar cells, with special focus on the photochemical processes occurring in the active layer. She is currently a postdoctoral scientist at Belectric OPV GmbH working on the incorporation of carbon nanotubes in organic solar cells within the FP7 Project "POCAONTAS".

Andreas Distler obtained his degree in chemistry and PhD from the Friedrich-Alexander University of Erlangen-Nuremberg (Germany) in cooperation with Konarka Technologies GmbH working on degradation mechanisms in polymer-fullerene solar cells. Since May 2014 he has been leading the research and development department as Director of R&D at Belectric OPV GmbH, the global market leader for OPV modules and installations.

Larry Lüer received his PhD from Tübingen University, working on oxygen effects on photoconductivity in small molecules. In 2001, he went to CNR/INFM Politecnico di Milano to work in the groups of Guglielmo Lanzani and Giulio Cerullo, applying femtosecond ultrabroadband pulses to study energy and charge transfer phenomena in conjugated oligomers and carbon nanotubes. He became senior researcher in 2003. Since 2009, he is senior researcher at IMDEA Nanoscience, Madrid, studying the photophysics of natural and artificial light harvesting systems.

2. Elementary Processes Causing Electrical Performance Loss in OSCs

2.1. Electrical Characteristics of OSCs

In order to understand how degradation causes electrical performance loss in OSCs, it is useful to start with a short introduction into general loss channels in OSCs. The power conversion efficiency (PCE or η) is defined as the maximum electrical power output (P_{out}) divided by the incident solar irradiation power (P_{in}), usually measured under standardized

conditions (i.e., 1000 W/m^2 irradiance, AM 1.5 spectral distribution, and 25 °C cell temperature):

$$PCE = \eta = \frac{P_{out}}{P_{in}} = V_{OC} I_{SC} FF / P_{in} \quad (1)$$

where V_{oc} is the open circuit voltage, I_{SC} is the short circuit current, and FF is the fill factor, defined as

$$FF = \frac{V_{mpp} I_{mpp}}{V_{OC} I_{SC}} \quad (2)$$

where V_{mpp} and I_{mpp} is the voltage and current, respectively, at the maximum power point (MPP). With OSCs integrated in a module, a so-called MPP tracker will adjust the load resistance (R_L) so that $R_L = V_{mpp}/I_{mpp}$, under the current irradiation conditions (hence, the definition of PCE via the electrical power at the MPP). We can formally understand the solar irradiation power as an incoming flux J_{ph} of photons of average energy E_{ph}^{av}, yielding

$$PCE = \frac{E_{OC} J_{SC}}{E_{ph}^{av} J_{ph}} FF. \quad (3)$$

Herein, $J_{SC} = I_{SC}/q$ is the flux of electrons and holes in the external circuit, $E_{OC} = V_{OC}q$ is the limit of the energy of the charges in the external circuit under open circuit conditions, and q is the elementary charge. Equation (3) allows us to express PCE as a product of efficiencies:

$$PCE = \eta_e EQE \quad (4)$$

with $\eta_e = E_{OC}/E_{ph}^{av}$ as the energy conversion efficiency, and $EQE = J_{SC}$ FF$/J_{ph}$ as the external quantum efficiency. In all types of solar cells, the energy conversion efficiency is reduced whenever an absorbed photon possesses a higher energy than the one of the respective transport state in the active layer, the excess energy then being released to the lattice as heat. In organic solar cells, η_e is additionally reduced by the energy needed to dissociate the strongly bound excitons and by friction losses in the low mobility organic phases.[11]

Active layer degradation can affect both η_e and EQE. A reduction of PCE by up to 25% during the initial phase of illumination has been described for various blends, mostly by a reduction of FF and V_{oc} (and thus η_e).[12] As oxygen has shown to contribute to this effect, it was investigated whether the V_{oc} loss has its origin in a change of the energy of the interfacial charge transfer state E_{CT}. It was however found that E_{CT} did not show any oxygen influence. For this reason, the loss in V_{oc} was ascribed to a reduced carrier density under open circuit condition, because both quantities are related via the Shockley equation.[13] The reduced carrier density can be caused, for instance, by traps, increasing the recombination yield.

A reduction of EQE can be caused either by reducing the FF or J_{sc}, or both.[14] It is therefore useful to understand the relation of these crucial and easily measurable parameters to specific loss processes. Considering the elementary processes in organic photovoltaics, we can express EQE as a product of individual quantum yields for light absorption, generation of free charges and charge extraction:

$$EQE = \phi_{abs} \phi_{gen} \phi_{extr}. \quad (5)$$

Thus, during the course of OSCs degradation, EQE can be reduced by individual loss processes causing either absorption, generation, or extraction losses.

2.2. Absorption Losses

Absorption losses will occur if the absorption spectrum of at least one of the absorbing components changes so that less excitons are produced within the active layer. This can be caused either by degradation of the π-conjugation in the donor material, reducing the ability of the material to absorb in the visible spectral region[15] or by morphological changes such as formation of large crystallites causing total absorption of the crystallites and reduced absorption in the depleted regions.[16] Generally, absorption losses become significant only after severe degradation where electrical performance losses exceed 80% and are usually overwhelmed by the contributions from other loss channels, see below.[15] As absorption losses reduce the amount of extractable charge carriers, their direct effect on the electrical performance is to reduce J_{sc}; however, if the reason for the absorption losses is morphological changes, then changes of the FF can occur in parallel.

2.3. Generation Losses

The formation of free, extractable charge carriers requires a cascade of individual processes, each proceeding with a rate high enough to outperform all respective competitive processes:

$$D^* + A \xrightarrow{\varphi_{diff}} D^* A \xrightarrow{\varphi_{CT}} \left(D^+ A^-\right) \xrightarrow{\varphi_{sep}} D^+ \ldots A^-; \phi_{gen} = \varphi_{diff} \varphi_{CT} \varphi_{sep}. \quad (6)$$

Excitons formed in the bulk of the donor(D)- or acceptor(A)-rich regions will have to diffuse to the D–A interface for efficient exciton dissociation. Typical exciton diffusion lengths in donor polymers are on the order of 10 nm.[17] In consequence, the yield of excitons diffusing to the D–A interface will drop below unity if the dimensions of the D- or A- rich phase exceed the exciton diffusion length, or if defect states, able to quench the exciton, are present at a molar fraction that is comparable to the reciprocal of the number of sites visited (NSV) during diffusion.[18] Note that due to the stochastic nature of exciton diffusion, NSV will be much higher than the number of sites on a hypothetical trajectory towards the interface "as the crow flies", so that even a small number of defects can reduce the exciton diffusion yield φ_{diff} significantly.

If diffusional motion has brought the excitons close enough to the D–A interface, such that a significant amount of wavefunction overlap is present between D and A, then charge transfer from D towards A follows modified Marcus theory and can be as fast as 45 fs.[19] The driving force for this charge transfer reaction to proceed at a high yield φ_{CT}

is the free energy loss from the neutral bound exciton D* to the charge separated state [D^+A^-]. Given the strongly bound nature of the neutral singlet excitons (caused by low dimensionality and low dielectric constant of typical organic compounds), the requirement of free energy loss can only be achieved by admixture of a sufficiently strong electron accepting material.

From the above it follows that if an exciton is created close enough to the D–A interface, then immediate exciton dissociation can take place without diffusive steps. The ratio of ultrafast to diffusion-mediated exciton dissociation is then related to the total D:A interfacial area; indeed it has been shown that the amount of ultrafast (sub-100 fs) exciton dissociation is reduced under conditions that favor domain size growth such as annealing.[17b,20]

Electron transfer phenomena require wavefunction overlap of the species involved. Therefore, exciton dissociation results in the formation of an interfacial, bound charge transfer state [D^+A^-]. In order to achieve mobile charged states that can be extracted under a built-in field, this bound charge transfer state must separate into individual D^+ and A^- states. The charge separation yield ϕ_{sep} depends on the relative rates for charge separation and charge recombination. A high rate of charge separation requires a free energy loss during this process despite the fact that the Coulomb binding must be overcome. Several scenarios have been invoked to provide this additional free energy. i) Hot exciton dissociation. Grancini et al. have described hot exciton dissociation at higher exciton energies in the system poly[2,6-(4,4-bis-(2-ethylhexyl)-4H-cyclopenta [2,1-b;3,4-b′]dithiophene)-alt-4,7(2,1,3-benzothiadiazole)] (PCPDTBT):$PC_{60}BM$.[21] Other authors found the contribution of hot exciton dissociation to be small.[22] ii) Contribution of disorder. Guo et al. found in annealed poly(3-hexylthiophene) (RR-P3HT):phenyl-C_{60}-butyric acid methyl ester ($PC_{60}BM$) films that there is no ultrafast charge generation if excitons are created in the ordered phase of P3HT; they concluded that there is no direct interface between the ordered phase of P3HT and the A-rich region.[17b] This picture is plausible because contact with A will disturb the long-range order of the P3HT phase; it is therefore to be expected that the D–A interface is amorphous. Since charge carriers possess lower energy in the ordered phase, the transfer of a positive charge from the amorphous D–A interface into the ordered bulk would supply the necessary free energy for this process to occur quickly. iii) Electron or hole delocalization in the charge transfer exciton can lead to a significant effective electron-hole separation, making charge separation a process which is within kT and therefore very fast.[23]

The opponent to charge separation is back electron transfer. The rate at which this process occurs, depends on the availability of a neutral state with an energy similar to the one of the charge transfer exciton. If the donor is a low bandgap polymer, frequently triplet states have adequate energy, so that triplet generation from recombination of charge transfer excitons can be a very efficient loss process.[24] If triplet states are not available, then recombination into a hot ground state is possible, albeit at a lower rate.

Separated charged states, D^+ and A^-, move independently under the influence of an electric field (drift) and concentration gradient (diffusion). If D^+ and A^- encounter each other at the D–A interface, then the charge transfer exciton is regenerated, and recombination into triplets or hot ground states can occur. If the recombining pair of charges originates from the same exciton dissociation event, the process is called geminate recombination, while if positive and negative charge stem from different generation events, it is called non-geminate recombination. We highlight that this is a purely kinetic definition. Although both recombination types are bimolecular and should therefore show a concentration dependent lifetime, in geminate recombination the lifetime does not depend on the charge concentration – the recombination rate of charges from the same geminate pair is not influenced by whether or not there are other geminate pairs. Pump-intensity dependent charge dynamics are therefore a means to distinguish between geminate and nongeminate recombination. However, kinetically we cannot distinguish whether the geminate pair recombines after being separated and subject to diffusion for a period of time (this is the Onsager-Noolandi-Hong model),[25] or whether the charge transfer exciton has not been separated at all and disappears "in place".

It has been shown in P3HT:$PC_{60}BM$ blends that annealing greatly reduces the amount of geminate recombination,[20] which has been explained by the increase of charge separation pathways upon thermally induced crystal growth, while in as-deposited P3HT:$PC_{60}BM$ films the crystallites are so small that positive and negative carriers remain spatially correlated, increasing the geminate recombination probability. The direct effect of generation losses on the electrical performance is always a reduction of J_{sc}. However, note that the underlying mechanisms causing such generation losses often entail morphological changes that can influence the FF as well.

2.4. Extraction Losses

There is only one opponent to charge extraction, namely nongeminate charge recombination. for which we can write the recombination rate as

$$\frac{dn}{dt} = \frac{dp}{dt} = -k_r(n,p)\,np. \tag{7}$$

The rate coefficient $k_r(n,p)$ depends on the carrier concentration because in the framework of Langevin recombination, it depends on the charge mobility. In low mobility organic semiconductors, charge mobility is accomplished by single, stochastic charge transfer ("hopping") steps; for this reason the available density of states (DOS) distribution controls the hopping rate. Typically, charge mobilities increase when the occupation of the DOS is increased, i.e., at higher charge densities.[26] However, it has recently been shown that the charge density dependence of mobility can be only apparent and caused by spatial separation of positive and negative carriers under open circuit conditions.[27] Setting n = p (only photoinduced carriers) and using a dispersive ansatz, $k_r(n) = k_r^0\, n^\gamma$, for the dependence of the reaction rate on the carrier density, we can restate Equation (7) according to

$$\frac{dn}{dt} = -k_r^0 n^\gamma n^2 = -k_r^0 n^{2+\gamma} = -k_r^0 n^\xi \quad (8)$$

where $\xi = 2+\gamma$ is the kinetic reaction order, which is typically found between 2 and 3.[28] Thus, the charge recombination rate depends strongly on the concentration of charges. High extraction yields can therefore be achieved by keeping the stationary charge carrier density as low as possible. Conversely, an excess charge carrier density causes extraction losses by favoring recombination. Accumulation of charges (and thus, extraction losses) can be caused by a variety of mechanisms:

- Low mobility of one carrier type. The drift velocity depends linearly on the charge mobility, as does the extraction time. Long extraction times thus increase the stationary charge density and reduce the extraction yield. The accumulation of excess-non-equilibrium carriers causes a splitting of the quasi-Fermi levels in the device, with the severe consequence that the potential drop across the active layer is much less than the applied voltage; the resulting very low drift velocities are the main reason for the reduction of the extraction yield.[11c] This mechanism is behind the electrical performance loss caused by $PC_{60}BM$ dimerization.[6] Also photo-oxidative defects can reduce the charge mobility, causing extraction losses.[14b]
- Low extraction field. The presence of "background carriers" e.g., from an autoionization equilibrium involving defect states, can shield the built-in field in large portions of the active layer. The resulting charge accumulation will cause strong recombination and a reduced extraction yield.[14b,29]
- Delamination. Weak interaction between the hydrophobic active layer and the selective contacts which are typically hydrophilic, will cause a barrier for charge extraction over time or even a literal fracture of part of the device area.[30]
- Even in the absence of physical delamination, restricted charge transport across interfaces (between active layer and selective contacts) can cause space charges which act as a second diode in series with the OSC architecture, causing typical "S shapes" frequently observed in *J–V* curves.[31]
- Lack of percolation paths towards selective contacts. Thermodynamically controlled morphological evolution of the active layer can result in island formation inhibiting extraction of charges formed on the islands. Another phenomenon commonly observed is vertical demixing (stratification along the stack direction) of D- and A rich phases.[16] If the D-rich phase accumulates near the electron extraction layer, it will cause an accumulation of electrons in the A-rich phase, not finding percolation paths towards the selective contact, which will cause extraction losses.
- Both geminate and nongeminate recombination rates can be accelerated by orders of magnitude if there is a triplet state below the energy of the charge separated state. This has been found for a series of low-bandgap polymers, especially from the silaindacenodithiophene (SiIDT) class,[32] and from the diketopyrrolopyrrole (DPP) class.[33] This mechanism severely depresses the achievable J_{sc} values from such devices. It has been shown that blending low-bandgap polymers with a third phase taking over the role of a hole transporter, can protect the charges from rapid recombination while retaining the high absorption yield of the low-bandgap polymer.[34]

As extraction losses are caused by recombination which in turn depends on the stationary carrier density, extraction losses will be high at the MPP, and therefore cause predominantly a FF loss. However, often the stationary carrier density under short circuit conditions is still sufficient to cause recombination losses; in these cases a concomitant drop in J_{sc} is observed. Delamination can cause both FF and J_{sc} losses, depending on the precise mechanism and on the size of the defects. If the delaminated regions are large enough, delamination can act predominantly on J_{sc}, because it essentially reduced the active device area where charges can be extracted. Since in large delaminated areas, the resulting barrier cannot be overcome by a strong reverse bias, such areas do not cause an FF drop and will behave as a generation loss although mechanistically they are extraction losses.[4a]

2.5. Mechanistic Studies

In order to understand and tackle OSCs degradation, it is important to determine which of the above mechanisms is responsible for the observed electrical performance loss. On the one hand, it has been shown that degradation investigations on isolated active layers are a valid and powerful method to predict the stability of the respective solar cells.[6a,35] On the other hand, inspection of *J–V* curves of complete photovoltaic devices gives the most important qualitative insight: as detailed above, the observation of FF losses upon degradation definitely points to enhanced recombination. The observation of an "S shape" in the fourth quadrant, with an inflection point close to the Voltage axis, points to an extraction problem between the active layer and one of the selective contacts. The resulting space charge region acts as a diode in series with the organic semiconductor, pushing the MPP to very low voltage values.[11b,31] A reduction of J_{sc} however is unspecific as all the above processes cause it to some extent. Efforts are therefore directed towards reproducing *J–V* curves, either by applying an equivalent circuit model,[36] or by using input parameters obtained from transient studies such as transient photovoltage/photocurrent (TPV/TPC).[37] Recently, it has been shown that charge accumulation must be taken into account at typical mobility values found in active layers of OSCs. An analytical formula is presented that accurately reproduces *J–V* curves from numerical drift diffusion calculations over a wide range of mobilities and light intensities.[11c] Thus, one can check whether the observed J_{sc} reduction is a consequence of FF reduction, or whether generation losses must be invoked as additional factor.

Some loss processes for extractable charges occur on the lower picosecond or even femtosecond time scale, e.g., trap-induced exciton deactivation or ultrafast triplet formation. The quantification of these processes requires a higher time resolution than possible with electronic circuitry, and it requires the detection of the time evolution of both neutral and charged excited states. The method of choice is therefore femtosecond transient absorption (TA) spectroscopy,[15,17a] tracing excited

state dynamics by measuring the time evolution of specific optical probes using the Beer-Lambert law:

$$\Delta A(\omega,t) = d\sum_{i=1}^{N}\sigma_i(\omega)c_i(t) \quad (9)$$

where the index i refers to the kind of excited state (singlet, triplet, charge in D-rich phase, charge in A-rich phase etc.), N is the total number of different kinds considered, $\sigma_i(\omega)$ is the cross-section spectrum of state i as function of probe energy $\hbar\omega$, and $c_i(t)$ is the concentration of state i as function of pump-probe delay time t. Applying appropriate matrix decomposition techniques to Equation (9), the dynamics $c_i(t)$ of several interacting species can be obtained by a global fit of measurements under different conditions (pump intensity, polarization of probe against pump pulse),[38] although it often helps to provide the cross-section spectra by additional measurements that are specific to one kind of excited states only, e.g., by performing charge modulation spectroscopy (CMS) for optical probes of charged states,[39] or adding a triplet sensitizer like, palladium-anthra-porphyrin.[33] Having obtained the time-resolved concentrations $c_i(t)$ of all relevant species, one can obtain yields for the various loss processes thus identifying the dominant mechanism for generation loss.[40]

One serious criticism of femtosecond spectroscopy is the high flux of the pump pulses during excitation, often exceeding GW cm^{-2}, which is 10 orders of magnitude above a typical solar flux. It is therefore essential to make sure that the pump pulse induces an excited state composition equivalent to the one caused by solar irradiation. This entails (i) avoiding nonlinear processes such as two-photon absorption and sequential excitation and (ii) producing a starting concentration of excited states equivalent to the stationary concentration under solar irradiation. For charged states, the latter requirement is manageable, as typical solar charge densities cause a transient absorption of around 10^{-4} in the band maximum which can be handled by modern TA systems.[41] Under these conditions, usually also requirement (i) is fulfilled. For excitons in contrast, the adjustment of requirement (ii) is impossible; due to their very short lifetimes, stationary exciton densities under solar irradiation all but vanish. The only way out is therefore to measure over a large range of pump intensities and do a kinetic analysis to disentangle high-intensity from low-intensity processes. This procedure has been applied successfully;[33,34] the quantification of high-intensity processes such as exciton – exciton annihilation provides additional insight into the mobility and diffusion length of the excited states.[42]

In order to distinguish between the various mechanisms that lead to FF losses, various techniques have been deployed that have spatial resolution along at least one direction. Deactivation and surface passivation can be traced in a destruction-free way by techniques with lateral resolution such as laser beam induced currents (LBIC).[43] Demixing and crystal growth in the active layer can be traced by measuring the neutron reflectivity,[44] and by X-ray diffraction (GIWAXS/GISAXS).[45] The latter two processes are also able to address a distribution gradient (stratification) along the stacking direction.

In **Figure 1**, we summarize this section by presenting a flow chart for a differential analysis of prominent loss channels in OSCs. It is not exhaustive but rather meant to present an overview of methods that are able to provide detailed enough insight to be able to devise targeted solutions to improve OSCs

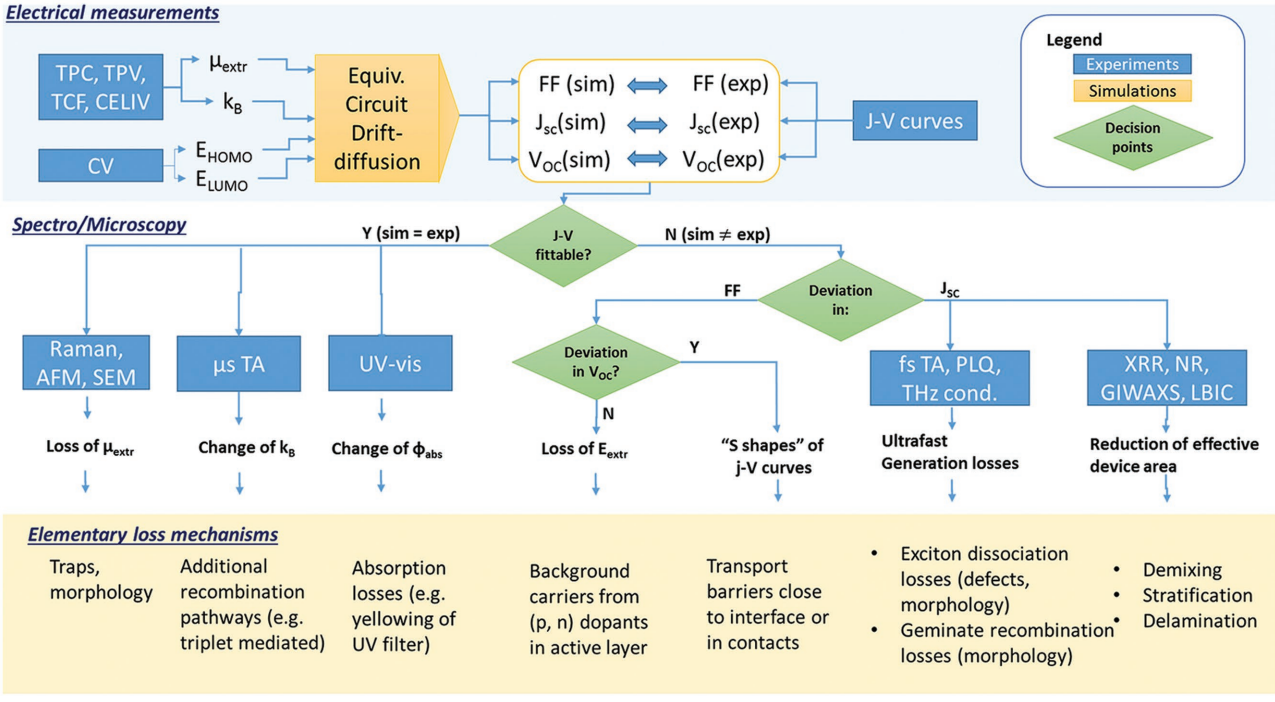

Figure 1. Differential diagnostic scheme to identify prominent loss and degradation channels. Upper row: Simulated and measured device data are calculated and compared. Middle row: Depending on success of electrical simulation, spectroscopic and microscopic studies are performed to identify the dominant loss channel. In the lower column, the most probable elementary mechanisms causing the loss are summarized.

lifetimes. The analysis always starts by inspecting the *J–V* curves of pristine and degraded devices, showing whether the PCE losses stem predominantly from losses of FF, J_{sc} or V_{oc}, or from a combination of these factors. Next, transient electrical measurements like, transient photocurrent/ transient photovoltage Time-resolved collection field or Charge Extraction by Linearly Increasing Voltage (TPC, TPV, TCF, CELIV, respectively) are performed to characterize charge recombination and extraction. These data, together with oxidation/reduction potentials of the active layer which are usually available from cyclovoltammetry (CV) done in the synthetic labs, can be fed into drift/diffusion and equivalent circuit simulations, in order to simulate the experimental *J–V* curves. If this works (left part in Figure 1), then device degradation follows the model deployed in the *J–V* simulations. According to whether the simulations attribute the dominant loss to μ_{extr}, k_b or φ_{abs}, further spectroscopic and microscopic studies can be deployed to reveal the elementary mechanism behind the extraction, recombination and absorption losses, respectively.[11c] If the simulations fail to reproduce either FF or J_{sc} (left or right path in second decision point, respectively) then additional mechanisms have to be considered that are not in the simulation model. In the case of underestimated FF losses, an additional series resistance must be assumed, caused either by degradation-induced background carriers in the active layer, or by transport barriers close to the interface or in the contacts; these phenomena can be distinguished by looking at the predicted V_{oc} loss (see decision points in right half of Figure 1. Finally, if J_{sc} (exp) ≠ J_{sc} (sim), then there are additional phenomena reducing the extractable current density: these can be ultrafast processes that cause a reduced production of extractable charges, or interfacial changes that reduce the effective area of the device. Only advanced spectro/microscopic techniques can distinguish between these possibilities.

3. Degradation of the Active Layer

This chapter treats the two main routes for active layer degradation: on one hand, the π-conjugated systems can be easily destroyed by photochemical reactions, especially in the presence of atmospheric oxygen. As a consequence, the absorption and charge transport properties of the materials are strongly affected, which directly leads to a loss in OSCs performance. On the other hand, the metastable nanostructure of the bulk-heterojunction giving best electrical performance has usually a tendency to evolve towards larger donor-and acceptor-rich regions, especially under the elevated temperatures encountered under solar irradiation, deteriorating the electrical performance of the cell.

3.1. Photochemical Changes

3.1.1. Photooxidation

The presence of molecular oxygen generally leads to a fast performance reduction of illuminated organic solar cells. For P3HT:PC_{60}BM and short irradiation times, it has been shown that this degradation is partly reversible upon annealing.[29] After longer irradiation times, irreversible photooxidation becomes dominant.[15]

Reversible Effects of Oxygen: Let us first discuss the reversible oxygen effect on device performance. The fact that electrical performance losses due to photooxidation of P3HT:PC_{60}BM cells can be partially reversed at 120 °C indicates that this reversible part cannot be attributed to covalent bond formation and cleavage. Seemann et al. have shown by experiments of charge extraction under a linearly increasing voltage (CELIV) that molecular oxygen, especially when illuminated, causes a doping of the active layer.[29] Simulations of the excess carrier distribution resulted in a quenching of the extraction field in large regions of the active layer, thus explaining the reversible J_{sc} reduction. The formed species that is responsible for this effect is found to be a metastable charge-transfer complex between P3HT and molecular oxygen that comprises mobile holes being delocalized over the polymer backbone and immobile electrons being trapped on the superoxide anion.[46] In pure P3HT films without acceptor, a reversible effect of molecular oxygen on the picosecond dynamics of singlet excitons and polarons has been shown.[17a]

Irreversible Effects of Oxygen: Prolonged exposure of OSCs to oxygen and light leads to irreversible degradation of the active layer. In P3HT:PC_{60}BM devices, a loss of optical absorption in the S_0-S_1 transition is observed,[15] pointing to changes in the conjugated π-backbone of the donor polymer as one reason for electrical performance loss. In order to clarify whether the reaction between molecular oxygen and the conjugated backbone proceeds via a radical pathway or via a sensitized pathway involving highly reactive singlet oxygen, photodegradation studies of pure P3HT films were performed.[9c,d,47] It was found that (i) the photodegradation proceeds at approximately constant rate (0^{th} order kinetics) and (ii) the action spectrum of the photodegradation rate does not follow the absorption spectrum of P3HT but increases by up to a factor of 50 in the near ultraviolet spectral region. Both findings make a radical pathway highly plausible, while ascribing only a minor role to singlet oxygen in the photooxidation of P3HT in the solid state. Nevertheless, reaction with singlet oxygen has been reported for other p-type polymers commonly employed in organic solar cells.[48] Whether a polymer is predominantly degraded via a mechanism involving singlet oxygen or oxygen centered radicals depends on the characteristics of the polymer itself and the degradation conditions, being different in the solid state or in solution,[48a,49] and depending also on the nature of the photons irradiating the sample.[9d]

However, the absorption reduction in the visible range caused by photooxidation of the donor polymer cannot explain the respective amount of irreversible performance reduction in the OSCs: in devices of P3HT:PC_{60}BM and Si-PCPDTBT:PC_{60}BM, a few percent of absorption reduction already cause an irreversible J_{sc} loss of 75%.[14b] Transient absorption studies in the femtosecond to millisecond time domains confirmed the absence of generation losses. This finding does not contradict the earlier works of Deschler et al.,[15] finding generation losses only upon much higher levels of photooxidation. Irreversible OSCs performance loss due to photooxidation must therefore be attributed to charge extraction losses.

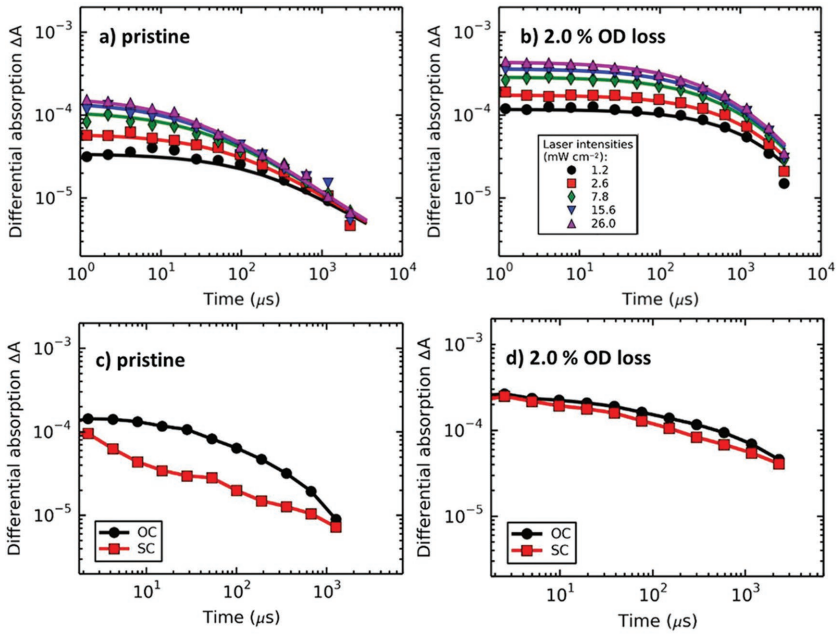

Figure 2. Transient absorption (TA) dynamics in P3HT:PC60BM devices, probed at 970 nm (charge induced absorption band in P3HT), at different levels of photooxidation, as indicated. a) and b) TA dynamics under open circuit conditions, after illumination by a 532 nm CW laser for 5.5 and 83.3 ms, respectively, at a repetition rate of 91 and 6 Hz, respectively, at intensities as given in the inset of panel (b). Time t = 0 refers to the moment of light off. c) and d) TA transients after 300 ps pulses at 532 nm and 1.83 μJ pulse energy, under short circuit and open circuit conditions (SC and OC, respectively). Adapted with permission.[14b] Copyright 2015, The Royal Society of Chemistry.

Microsecond transient absorption studies under variation of the pump intensity were performed to understand the nature of the extraction losses, see **Figure 2**. A degradation-induced cross-over from bimolecular recombination (known for pristine devices)[41] towards a pseudo-first order rate law was observed, compare Figure 2a and b, respectively. Given the fact that charge recombination is always bimolecular (requiring the encounter of two species to take place), the observation of a pseudo-first order rate can only be explained by a large excess of one carrier type with respect to the other. By globally fitting the decay traces to a rate equation model solved numerically, the amount of excess carriers was found to sharply rise and the bimolecular recombination coefficient was found to drop for increasing levels of degradation. In the framework of Langevin recombination, a reduction of the bimolecular recombination coefficient is caused by a lower charge mobility, so part of the extraction losses was ascribed to a mobility reduction leading to charge accumulation and enhanced recombination as indeed could be demonstrated. However, especially for the system P3HT:PC_{60}BM, a mobility reduction was considered not sufficient to explain the strong J_{sc} reduction upon photooxidation. In Figure 2c and d, charge transients are shown under open circuit (OC) and short circuit (SC) conditions, for the pristine and degraded device, respectively. It becomes evident that the transients under both OC and SC conditions are strongly slowed down upon photooxidation. However, the effect is much stronger under SC than under OC conditions, which means that charge extraction is penalized more strongly than one would expect if only the mobility changed. This finding is in agreement with a reduced extraction field caused by the excess carriers from the photoinduced defects.[14b] This mechanism is similar to the one found by Seemann et al.,[29] only that here the excess carriers are prospectively caused by a yet unknown redox couple involving defect sites from the irreversible photooxidation.

3.1.2. Light-induced Changes in Absence of Oxygen

The negative effects of illumination in presence of extrinsic triggers such as oxygen and water can be avoided to some extent by the use of more favorable device architectures,[4a,50] materials,[51] and specially encapsulation.[10,52] Indeed, the electrical performance of OSCs is affected by the presence of these extrinsic triggers to such an extent that device stability (and cost) can be ultimately determined by the quality of the employed encapsulation materials. However, in certain cases, device performance losses can emerge from mere exposure to light. Frequently reported in the literature is the so-called "burn-in" process, characterized by an initial a rapid decay in efficiency which then flattens to a slower linear decay at later times.[6,12,53] Concerning the materials in the active layer, the absence of oxygen does not guarantee that photochemical reactions are fully prevented.[7a] Indeed, certain low bandgap polymers possess chemical bonds that can be homolytically broken via light absorption, for instance C—N or C—O bonds.[7d,9b,54] In turn, this creates free radicals that can further degrade the active layer.[7e] Related to this, material impurities or defects resulting from synthesis, which can be quantified by means of Electronic Paramagnetic Resonance,[55] can also lead to lower polymer photostability.[56] Furthermore, the fullerene can also undergo photochemical changes under illumination, which have been related to the aforementioned "burn-in" process.[6,53a] This topic is examined in detail in section 4.1.3.

3.2. Morphological Changes

The nanoscale morphology of the active layer of an optimized OSCs, the so-called bulk heterojunction (BHJ), is a bi-continuous network of D- and A-rich phases presenting the best compromise between two contradicting requirements: (i) the D- or A- rich regions should be small enough for all excitons to reach the D–A interface before being quenched by radiative or nonradiative processes, and (ii) they should be large enough to avoid charge recombination; as charge recombination occurs at the D–A-interface, the recombination rate is sensitive to the interface to bulk ratio, as has been rationalized

by Monte Carlo simulations.[57] This optimum nanostructure is, however, generally not the thermodynamically lowest state of the active layer; at elevated temperatures typical under device operation, the nanoscale morphology will therefore slowly evolve towards the thermodynamic equilibrium, causing electrical performance degradation. A prominent way of energy minimization in multi-phase solids is crystal growth according to the Oswald ripening mechanism.[58] It starts from nuclei that grow by depleting their neighborhood from the constituent molecules. As the depletion process is diffusion controlled, material uptake for the growing crystallites proceeds with the square root of time. These characteristics have been observed in BHJ solar cells made of poly(2-methoxy-5-(3′,7′-dimethyloctyloxy-1,4-phenylenevinylene) (MDMO-PPV):$PC_{60}BM$(1:4) in which the clusters of $PC_{60}BM$ have been shown to grow with the square-root of time during annealing using transmission electron microscopy (TEM), causing a concomitant drop in the short circuit current. This drop in J_{sc} was interpreted as generation loss, because the larger the crystals, the lower the fraction of excitons than can reach the D–A interface.[58]

As carrier drift occurs vertically, along the stack direction, the vertical D–A composition and its change following thermal treatment have received special attention. By means of X-ray reflectivity (XRR) measurements in P3HT:$PC_{60}BM$ films spin-coated from different solvents, clear evidence of stratification was observed which changed upon annealing.[59] Films spun from toluene, chlorobenzene, and xylene showed enrichment of $PC_{60}BM$ at the top and a depletion of $PC_{60}BM$ at the bottom, which is beneficial for OSCs in the conventional device architecture where electrons are extracted at the top. Recently, Chintala et al. have demonstrated vertical composition profiles by combining gas cluster ion beams and scanning probe microscopy thus avoiding the need of synchrotron radiation.[60] Preparing depth profiles using the ion beam and scanning $1 \times 1\ \mu m^2$ large regions of the samples by conductive atomic force microscopy (C-AFM), they found an increase of $PC_{60}BM$ content close to the surface, which coincides with the findings of Ruderer et al. Statistics over many $1 \times 1\ \mu m^2$ regions showed only little distribution. After annealing, the overall stratification was roughly retained but the standard error was greatly increased: at a certain depth, a P3HT:$PC_{60}BM$ ratio anywhere between 25% and 75% could be found, which is detrimental for charge generation. They found micrometer sized $PC_{60}BM$ hillocks, explaining this large standard error.[60]

4. The Role of Carbon Materials on the Degradation of the Active Layer

4.1. Fullerene Derivatives

4.1.1. Properties

Fullerene derivatives are commonly employed as electron acceptors in the active layer of OSCs, particularly [6,6]-phenyl-C_{61}-butyric acid methyl ester ($PC_{60}BM$).[61] The structure of fullerene C_{60}, depicted in **Figure 3**, is based uniquely on carbon atoms, arranged in 20 hexagonal and 12 pentagonal rings with icosahedral geometry (I_h). The high symmetry of this molecule is responsible for its favorable optical and electronic properties;[62] for instance, the capability of accepting up to six electrons,[63] or the small reorganization energy associated with most of their reactions.[64] Whilst the application of C_{60} as such in solution-processed solar cells is limited by its low solubility,[65] this problem has been successfully circumvented via the synthesis of soluble C_{60} derivatives bearing one or various addends, as $PC_{60}BM$,[66] bis-$PC_{60}BM$,[67] or indene-C_{60} bis-adduct ($IC_{60}BA$),[61,67] (see Figure 3). Furthermore, the number and type of substituents can be used to tune the electron affinity of the fullerene. Such modification of the energy levels can, in turn, enhance device performances (thanks to incremented V_{oc} values) or modify the stability towards photooxidation (this effect is further discussed in the next section).[6a,8b] Indeed, increasing the substitution in the fullerenes does also modify the steric hindrance of the molecules, this affecting both their reactivity,[6] and their molecular intercalation with polymer semiconductors.[68] Additionally, C_{70} derivatives (such as $PC_{70}BM$ or bis-$PC_{70}BM$, see Figure 3) display an enhanced absorption in the visible range (compared to C_{60} derivatives) due to lower symmetry of the fullerene cage, thus being able to increase the external quantum yield in solar cell devices.

The physicochemical characteristics of fullerenes determine their own reactivity and, as a result, their effect in the stability of organic solar cells. Under exclusion of light and oxygen, fullerene derivatives have been reported to be thermally stable up to several hundreds of degrees Celsius.[69] However, exposure of fullerenes to oxygen provokes the reversible intercalation of oxygen atoms, which can act as quenchers of fullerene singlet states,[13a] or traps reducing electron mobility.[70] Combined exposure to light and oxygen leads to both an enhanced diffusion of oxygen in the fullerene cage and irreversible oxidation processes, notably with formation of covalent bonds such as epoxides (C > O) or carbonyl bonds (C=O).[71] In absence of oxygen, light is able to trigger the polymerization of C_{60} and, to a lower extent, of C_{70}.[72] The fact that this reaction is effectively suppressed in presence of oxygen has led to the conclusion that it proceeds via fullerene excited triplet states.[73] The reaction mechanism of the dimerization has been postulated as a thermally reversible, [2+2] cycloaddition between two parallel 6-6 double bonds located on adjacent fullerenes.[6b,72d,73,74] Mono-substituted fullerenes, such as $PC_{60}BM$, have also been reported to dimerize upon illumination.[72c,75] The implications that such dimerization process has in solar cell performances are addressed in section 4.1.3. Indeed, in addition to the (photo) chemical processes occurring for the pure material, analysis of the role of the fullerene in the stability of the active layer needs for considering its blend with the electron donor, according to the widely employed bulk-heterojunction. In the following, stability of the active layer is discussed focusing firstly on the photochemical reactions taking place in presence of oxygen, and secondly analyzing the photochemical and morphological changes occurring under inert atmosphere.

4.1.2. Photooxidation of the Active Layer

Influence of the Fullerene Electron Affinity: Photooxidation of the active layer is a main cause for the drop in performances as

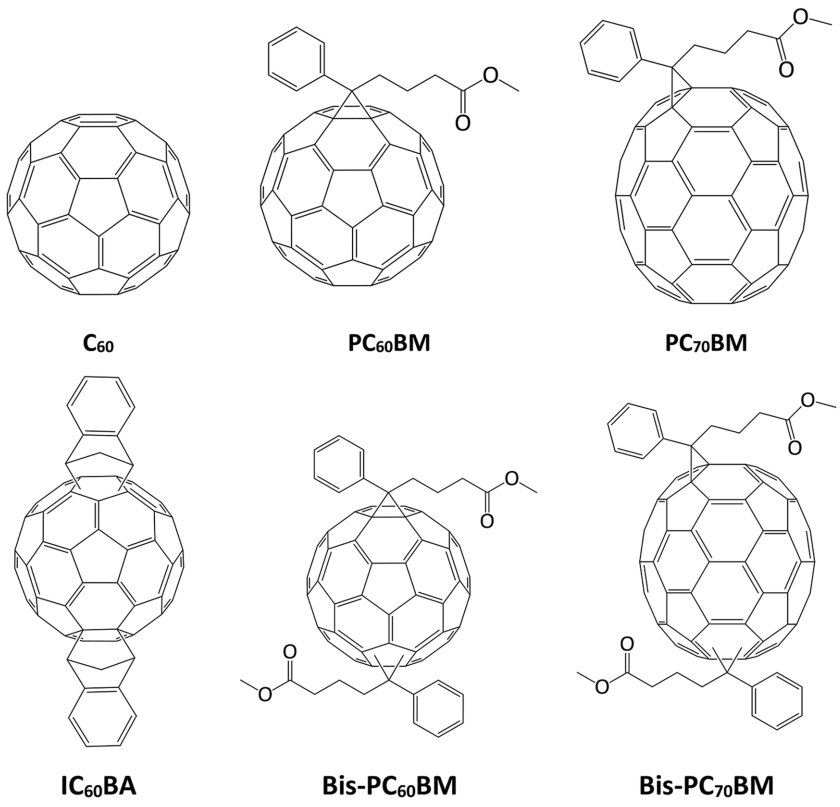

Figure 3. Structure of C_{60} and derivatives of C_{60} and C_{70}.

solar cells are irradiated in air.[29] In this process, the fullerene component is found to play a decisive role as it can impose both stabilizing and destabilizing effects on polymers upon photooxidation. The quality and extent of these effects depend both on the type of fullerene and polymer.[6a,7e,8a,b,76] Concerning the first, studies have related the electron affinity of the fullerene derivative to the extent of stabilization imparted by it.[6a,8b] Distler and co-workers have examined the illumination in air of P3HT films blended with C_{60}-based fullerenes with varying organic substituents and electron affinities ranging from −3.53 to −3.83 eV, including $PC_{60}BM$ (−3.70 eV).[6a] Whilst the degradation rate of P3HT was lower in all blends compared to that of the neat P3HT film, the stabilization factor imposed by each fullerene was dependent on its electron affinity. Accordingly, the extent of stabilization increased as the LUMO levels went down to −3.75 eV (maximum stabilization factor of 7.5); after which, stabilization decreased again for higher electron affinities (see **Figure 4**a). It is noteworthy that the degradation of solar cells based on these active layers showed the same dependency on the electron affinity of the fullerene as the degradation of isolated films (Figure 4a). This highlights the powerfulness of studies on separate active layer films as for predicting the lifetime of solar cells under these degradation conditions.

Similarly, Hoke et al. reported increasing photobleaching rates as P3HT was blended with fullerenes of lower electron affinity (see Figure 4b).[8b] This relationship between polymer photooxidation and the electron affinity of the fullerene would be in accordance with a mechanism of degradation involving photogenerated electrons. Accordingly, electronic transfer from the excited polymer or fullerene to molecular oxygen would form superoxide radical anions ($O_2^{\bullet-}$), able to then react and degrade the polymer. However, such electronic transfer from the fullerene to oxygen is only likely to happen with fullerenes of small electron affinities. Thus, whilst the overall lower photooxidation rates observed for all blends (compared to pristine polymers) were attributed to the radical scavenging abilities of fullerenes, it was suggested that the more electropositive fullerenes could also contribute to the formation of reactive $O_2^{\bullet-}$ and degrade the polymer.[8b] However, this explanation does not justify the increasing photooxidation rates above the threshold of 3.75 eV observed in Figure 4a. Further insight into the stabilizing and destabilizing mechanisms of fullerenes is provided in the next subsections.

Hoke et al. extended the study to different polymers, namely poly[2-methoxy-5-(3′,7′-dimethyloctyloxy)-1,4-phenylenevinylene] (MDMO-PPV), poly[2,5-bis(3-tetradecylthiophen-2-yl)thieno[3,2-b]thiophene] (PBTTT), and poly[[5-(2-ethylhexyl)-5,6-dihydro-4,6-dioxo-4H-thieno[3,4-c]pyrrole-1,3-diyl][4,8-bis[(2-ethylhexyl)oxy]benzo[1,2-b:4,5-b′]dithiophene-2,6-diyl]] (PBDTTPD), and obtained similar trends with the electron affinity in all cases (see Figure 4b). Additionally, not only stabilizing but also destabilizing effects (i.e., enhanced photooxidation rates) were observed for polymers blended with the more electropositive indene-C_{60} trisadduct ($IC_{60}TA$) and indene-C_{60} bisadduct ($IC_{60}BA$), see for instance results for MDMO-PPV in Figure 4b. Furthermore, whilst the trend of photooxidation rate with electron affinity was the same for all investigated polymers, the extents of stabilization/destabilization applied by the fullerene varied from polymer to polymer. In line with this, Distler and co-workers identified that the most frequently employed $PC_{60}BM$ can both accelerate and decelerate the photooxidation rate depending on the polymer it is blended with.[8a] Three different polymers, namely P3HT, poly[2,6-(4,4-*bis*-(2-ethylhexyl)dithieno[3,2-*b*:2′,3′-*d*]silole)-*alt*-4,7-(2,1,3-benzothiadiazole)] (Si-PCPDTBT), and poly[2,6-(4,4-bis-(2-ethylhexyl)-4H-cyclopenta[2,1-b:3,4-b′]dithiophene)-alt-4,7-(2,1,3-benzothiadiazole)] (C-PCPDTBT), were blended with $PC_{60}BM$ and the kinetics of photooxidation were compared to pristine films. The results indicated a strong to moderate stabilization for P3HT and Si-PCPDTBT, respectively, and an acceleration of the degradation by a factor of two for C-PCPDTBT. These results highlight that the mechanistic behind is not only determined by the fullerene itself but also by the polymer and its characteristics.

Fullerene Stabilizing Mechanisms: This section evaluates the mechanisms of stabilization and destabilization of $PC_{60}BM$ in the degradation of the active layer. Three main stabilizing mechanisms are discussed: excited state quenching, light-screening effect, and chemical effects (e.g., radical scavenging). As for destabilizing effects, these are related to the photosensitization

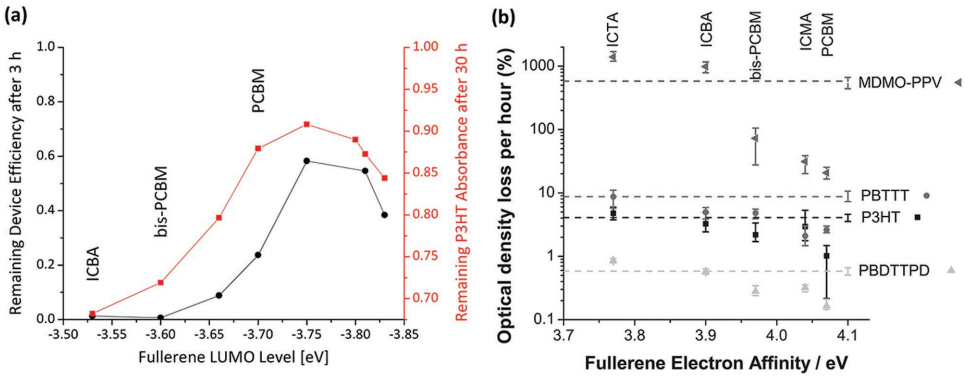

Figure 4. a) Maintained device efficiency (black) and remaining P3HT absorption (red) after irradiation under ambient atmosphere for 3 h and 30 h, respectively, in function of the fullerene LUMO levels. Reproduced with permission.[6a] Copyright 2015, A. Distler. b) Photobleaching rate of different polymer:fullerene films as a function of the fullerene electron affinity, where the dashed lines indicate the oxidation rate of pristine polymer films. Reproduced with permission.[8b] Copyright 2012, John Wiley & Sons. Note: comparing both graphs, the electron affinity scales differ in terms of a linear shift by a value of 0.37 eV (see indications for ICBA, bis-$PC_{60}BM$, and $PC_{60}BM$ for comparison).

of reactive oxygen species (such as singlet oxygen $^1O_2$, superoxide anion $O_2^{\bullet-}$, etc.) able to trigger polymer degradation.

A possible stabilization mechanism often referred in the literature is the quenching of polymer excited states by electron transfer to $PC_{60}BM$.[76a,b] After excitation, rapid exciton dissociation at the fullerene-polymer interface would reduce the stationary exciton density in the polymer, which in turn would diminish the rate of processes involving polymer excitons (e.g., direct reaction of singlet excitons with molecular oxygen or production of polymer triplet states). The influence of triplet states in the photooxidation of MDMO-PPV was examined by Chambon et al. by blending it with 1,4-siazabicyclo[2.2.2.]-octane (DABCO), an additive able to quench the triplet state of poly(phenylene vinylene).[77] Whilst the presence of DABCO indeed stabilized the degradation of the polymer, this occurred to a lesser extent than when MDMO-PPV was blended with $PC_{60}BM$. This finding indicates that the stabilization observed for MDMO:$PC_{60}BM$ blends must be due to an effect other than triplet quenching.[76d] Furthermore, similar extents of stabilization were observed for blends with $PC_{60}BM$ under both photo- and thermooxidative conditions, thus excluding excited species and rather pointing towards a radical mechanism. The role of excited-state quenching was examined by Hoke et al., who determined the photoluminescence quenching efficiencies for the polymer:fullerene combinations in Figure 4b.[8b] Although observing a degree of quenching above 95% in all cases, some blends degraded faster than the corresponding pristine polymers, thus indicating that decreasing the singlet state population was not the main route for stabilization. The same conclusion was reached by Distler et al. in their investigations about the role of $PC_{60}BM$ on the stability of different p-type polymers. In their study, the degree of (de)stabilization of $PC_{60}BM$ over P3HT, Si-PCPDTBT and C-PCPDTBT was compared to that imparted by the small molecule 2,7-dinitrofluorenone (DNF), which quenched fluorescence in the three polymers to approximately the same extent as $PC_{60}BM$. Despite the same quenching effect, DNF had a small stabilizing effect on all the polymers, whilst $PC_{60}BM$ affected both positively and negatively degradation of the studied polymers. The authors proposed that neither the fluorescent excited state nor the states derived from its decay processes are primarily involved in the photodegradation of the polymer. This conclusion is supported by the observation that the action spectrum of P3HT photo-oxidation does not coincide with the P3HT absorption spectrum.[47]

Oxidation of the polymer donor in the active layer is a photo-induced process, linearly dependent on light intensity and exhibiting a dependence on the type of photons.[47,78] Since fullerenes absorb mainly in the ultraviolet region of the spectrum, light-screening the polymer from these highly energetic photons is expected to account for a certain stabilization of the degradation. This effect has been quantified by comparing the degradation rate of a neat P3HT film, its blend with $PC_{60}BM$, and a third sample where the $PC_{60}BM$ layer was deposited on the opposite side of a glass substrate coated with P3HT.[8a] The results indicated that the degradation rate of the P3HT film screened by a $PC_{60}BM$ film was only 30% of the value observed in the P3HT:$PC_{60}BM$ blend. Additionally, the overall inner filter effect in the blend was proposed to be even lower (possibly < 15%), since only the very last layer of the film can be effectively filtered from irradiation to a same extent as the layer protected with a solid $PC_{60}BM$ film. Finally, whilst a certain stabilization of the polymer is observed in presence of $PC_{60}BM$, additional filtering of the UV wavelengths upon irradiation does result in an incremented stability of active layer films upon photooxidation.[78]

The radical scavenging ability of fullerenes is well-documented in the literature.[79] Accordingly, the fullerene ability to stabilize polymers in the active layer is frequently ascribed to its radical scavenging properties.[8b,76d,78] Evidence for radical scavenging stabilization mechanism has been obtained by finding similar oxidation products and extents of stabilization by $PC_{60}BM$ when the active layer was treated thermally or photochemically in presence of oxygen.[76d] Additional proofs for this mechanism have been obtained from the results obtained adding nickel(II)bisdibutyldithiocarbamate ($Ni(dtc)_2$) to the active layer.[6a] This compound is able to stabilize P3HT upon photo-degradation under ambient atmosphere, leading to an almost complete suppression of polymer degradation at early stages of irradiation (see **Figure 5**a). However, when added to P3HT already blended with $PC_{60}BM$, no additional stabilization

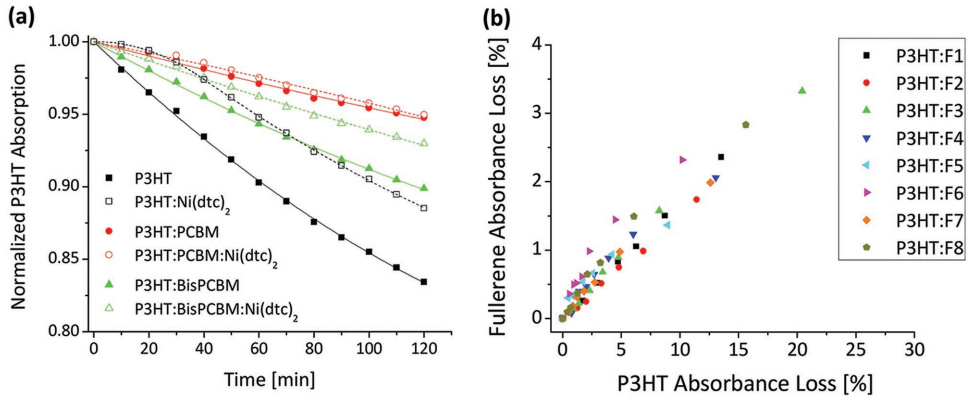

Figure 5. a) Normalized P3HT absorption upon photooxidation of P3HT (black), P3HT:$PC_{60}BM$ (red), and P3HT:bis$PC_{60}BM$ (green) pristine films and loaded with 10% of $Ni(dtc)_2$. b) Relative fullerene and P3HT absorption loss in blends of P3HT with fullerenes of different electron affinities exposed to irradiation in air. Reproduced with permission.[6a] Copyright 2015, A. Distler.

effects on P3HT were observed, this suggesting that the mechanism by which both components stabilize P3HT is the same. The Ni complex can act as stabilizer via different mechanisms, namely screening of UV light, singlet oxygen quenching, and free-radical scavenging and hydroperoxide decomposition.[80] Concerning the first, light screening was found to play only a minor role (also in line with the results mentioned above) compared to the other mechanisms.[80b] Although $Ni(dtc)_2$ is known to be an excellent singlet oxygen quencher both in solution and in the solid state,[80b–d] degradation of P3HT by means of singlet oxygen has been reported to occur in solution,[48a] but not in solid films, where a chain radical oxidation mechanism governs.[7b,49] Since these studies have been done in polymer films, the main stabilizing effect of $Ni(dtc)_2$ on P3HT in films cannot solely based on the quenching of singlet oxygen. Thus, the stabilizing effect shared by $Ni(dtc)_2$ and $PC_{60}BM$ was ascribed to their radical scavenging properties.[6a] Interestingly, the stabilization of the polymer by $Ni(dtc)_2$ leads to the own decomposition of the additive, whereas $PC_{60}BM$ and other fullerenes showed a non-sacrificial stabilization behavior (i.e., the slower P3HT degrades, the slower degradation of the fullerene occurs as well).[6a]

Figure 5b displays the relative loss of absorption for P3HT blended with fullerenes of different electron affinities. Whilst the electron affinity of the fullerenes affected the extent of stabilization imparted over the polymer, this plot shows a linear correlation between the degradation of P3HT and the different fullerenes, independently of LUMO level. It was then concluded that the radical scavenging ability of the fullerene moderates the steady-state concentration of oxygen-centered radicals, which, in turn are the main species responsible for degrading, to a same extent, both P3HT and fullerene in the investigated blends.[6a]

Fullerene Destabilizing Mechanisms: Photooexcitation of the active materials can sensitize the production of reactive oxygen species, which can contribute to the oxidation of the polymer and/or fullerene. Accordingly, electron or energy transfer from polymer or fullerene excited states to molecular oxygen can form superoxide radical anions ($O_2^{\bullet-}$) or singlet oxygen ($^1O_2$), the two main species reported responsible for the photooxidation of polymer donors in the active layer.[7a,d,e,9a,b,48,76d,78,81] Which of these species is predominantly degrading the polymer is somewhat controversial, as it depends on the characteristics of each specific polymer and the degradation conditions. For instance, whilst P3HT in solution is reported to degrade by means of singlet oxygen,[48a] this mechanism is discarded in polymer films in favor of a chain radical oxidation mechanism.[7b,49] On the contrary, poly(thieno[3,4-b]thiophene-alt-benzodithiophene) (PTB7), has been reported to degrade via singlet oxygen attack both in solution and films.[48b]

According to the discussion about excited state quenching, the main origin of the reactive oxygen species cannot be related to the direct photooexcitation of the polymer.[8a,b] However, formation of a charge transfer complex (CTC) between the polymer and oxygen ($P^+/O2^-$) has been reported to occur even in presence of the fullerene,[29,46,82] accounting for so-called reversible oxidation of the active layer.[29] Furthermore, the CTC with oxygen has been also associated with irreversible oxidation processes, for instance if the relaxation of the complex produces $^1O_2$ states.[83]

As for photoexcited fullerenes, they are able to transfer both energy[84] and electrons[85] to molecular oxygen to form reactive singlet oxygen ($^1O_2$) and superoxide anions ($O_2^{\bullet-}$), respectively. Aforementioned, the observation that P3HT (reported to degrade by a chain radical oxidation mechanism) degrades faster in blends with more electropositive fullerenes supports a radical degradation mechanism by means of $O_2^{\bullet-}$.[6a,8a] It seems plausible that there is a higher probability for the formation of superoxide via electron transfer from the fullerene to oxygen when fullerene LUMO levels are higher. In line with this, the oxidation rate of PPV polymers was shown to increase in blends with superoxide sensitizer 9,10-dicyanoanthracene.[9a,77] Additionally, the presence of water has been linked to increased photooxidation rates in P3HT,[47] which would be in line with the fact that hydrated forms of oxygen are easier to reduce than isolated O_2.[86]

After light-induced excitation of the polymer, ultrafast electron transfer to the fullerene takes place creating a so-called charge transfer complex (CTC) between the polymer and the fullerene (P^+/F^-), creating fullerene anions with yields close to unity.[20] Since the energy of F^- transient species is found in the range of the reduction potential of oxygen,[8b] electron transfer

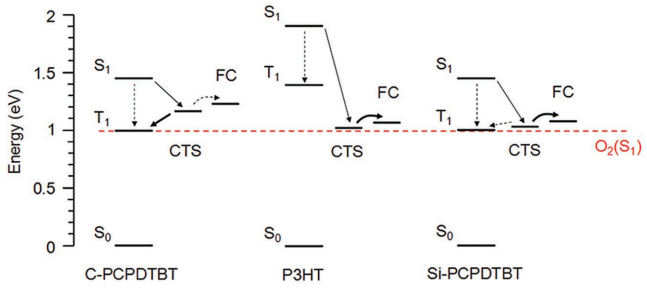

Figure 6. State diagram of C-PCPDTBT, P3HT and Si-PCPDTBT blends with $PC_{60}BM$ blends as proposed by Distler et al.[8a] CTS denotes the energy level of the charge-transfer state between the polymer and $PC_{60}BM$; and FC is the energetic level of free charge carriers. The dashed red line represents the energy of $^1O_2$. Reproduced with permission.[8a] Copyright 2012, American Chemical Society.

from the fullerene anion to molecular oxygen is also a plausible pathway for creating harmful superoxide anion species. This electron transfer would also be favored in the case of more electropositive fullerenes. Alternatively, when the energy levels are favorable, population of the polymer triplet state of the polymer from the CTS can occur (see **Figure 6**). Formation of polymer triplets is also possible via alternative routes, e.g., nongeminate polarons.[87] If the energy of the long-living triplet state lies above that the singlet oxygen state (0.98 eV), production of this reactive species can follow.

Remarkably, triplet state population from the CTS has been associated with enhanced photooxidation rates in the blend (compared to neat polymers), in C-PCPDTBT[8a] or PTB7.[48b,41b] However, the underlying reason for enhanced oxidation has been identified different in both cases. On the comparison among the effect of $PC_{60}BM$ over P3HT, Si-PCPDTBT and C-PCPDTBT, neat polymer films exhibited weak triplet signals, which were quenched upon addition of $PC_{60}BM$ for Si-PCPDTBT and P3HT (stabilized by PC60BM), but enhanced by up to 50% in the case of C-PCPDTBT. Furthermore, enhanced phase separation created by processing diiodooctane (DIO),[88] led to a lower extent of destabilization of the polymer by $PC_{60}BM$ due to a reduced formation of charge transfer states between the polymer and the fullerene, consequently decreasing the population of polymer triplets.[8a,89] It was then proposed that singlet oxygen sensitization could be the reason for an enhanced oxidation in the blend compared to the neat polymer, which was only possible in the case of C-PCPDTBT (see Figure 6).[8a] However, recent studies indicate that the triplet states in C-PCPDTBT do not play a role in the photodegradation of the polymer.[90] It was proposed instead that the photoexcited interfacial CT state does create reactive radical species ($O_2^{\bullet-}$) via electron transfer to contaminants in the sample ($^{\bullet}OH$, $^{\bullet}OOH$) or hydrated O_2.[90] In the case of PTB7 films, triplet population and production of singlet oxygen via charge transfer to molecular oxygen has been identified as the cause for their rapid oxidation.

4.1.3. Photodegradation of the Active Layer under Inert Atmosphere

In absence of oxygen, organic solar cells frequently suffer from a so-called "burn in" loss in device efficiency at early stages of irradiation.[6,12,53] Light-induced dimerization of the fullerene has been reported as the cause for this behavior, where the loss in performance is due to severe losses in short circuit current (J_{sc}) and fill factor (FF).[6b] Conversely, dimerization of $PC_{60}BM$ has been indicated to have a positive effect on solar cell stability, as it helps maintaining the morphology of the active layer when modest illumination is applied prior to (or upon) thermally stressing the devices.[91] The mechanism of $PC_{60}BM$ dimerization, the influencing factors and its implications on the solar cells performance and stability are subsequently described.

Dimerization of $PC_{60}BM$: Influencing Factors and Implications: Several techniques can be used to identify and monitor oligomerization in fullerene or blend films. Depicted in **Figure 7**b, the analysis of pristine $PC_{60}BM$ films using High-Performance Liquid Chromatography (HPLC) reveals one main signal attributed to $PC_{60}BM$ (and a minor signal of C_{60}). After light soaking, multiple additional signals appear at higher retention times, which correspond to the variety of regioisomers resulting from dimerization.[6b] When HPLC is coupled with Mass Spectrometry, further evidence for these traces corresponding to $PC_{60}BM$ dimers (m/z 1822 u) can be obtained.[53a] UV/Vis spectroscopy (Figure 7c) allows for readily monitoring dimerization either in neat $PC_{60}BM$ films or in blends with an adequate polymer donor, as illumination under inert atmosphere leads to an increment of the absorbance at 320 nm together with a slight blue-shift on the absorption at 335 nm.[6,53a] Additionally, the analysis of neat fullerene films using Raman or Fourier Transform Infrared (FTIR) spectroscopy allows for detecting the changes related to the dimerization (see Figure 7d,e).[91a,92] However, these two techniques are more difficult to implement for the analysis of polymer:fullerene blends due to the multiple and overlapping bands.[91c]

Valuable information about $PC_{60}BM$ dimerization has been obtained from the analysis of neat fullerene films.[6,53a] For instance, monitoring the increase in UV absorbance at 320 nm has been employed to acknowledge the influence of the type of fullerene (C_{60}-based or C_{70}-based, both mono- or bis-substituted) in the dimerization process. Whereas mono-substituted C_{60}-based fullerenes did show the characteristic rise at 320 nm, no changes were observed for all bis-substituted fullerenes (C_{60} or C_{70}) and C_{70} based fullerenes. The differential absorption spectra for the ensemble of fullerenes after irradiation are displayed in **Figure 8**a. Steric hindrance by the substituents is indicated as the cause for the absence of reactivity in multiple substituted fullerenes, as it also accounts for slowing down the kinetics of the photodimerization in mono-substituted fullerenes compared to plain C_{60}.[75a] In turn, the absence of dimerization in C_{70} derivatives is attributed to the presence of less reactive double bonds in the molecule.[72a,d] Interestingly, molecular packing in the fullerene phase does also play a role in the extent of dimerization. More crystalline $PC_{60}BM$ films impose geometric restrictions to the fullerene molecules,[53a,93] thus reducing the dimer content in the samples upon irradiation and yielding lower J_{sc} losses in devices fabricated accordingly.[53a] Concerning the influence of the ambient conditions, the reaction kinetics have been shown independent of the temperature in the range from 10 to 70 °C, indicating that this is not a diffusion controlled process.[6a] However, at temperatures above 100 °C, the retro-reaction from the dimer to the

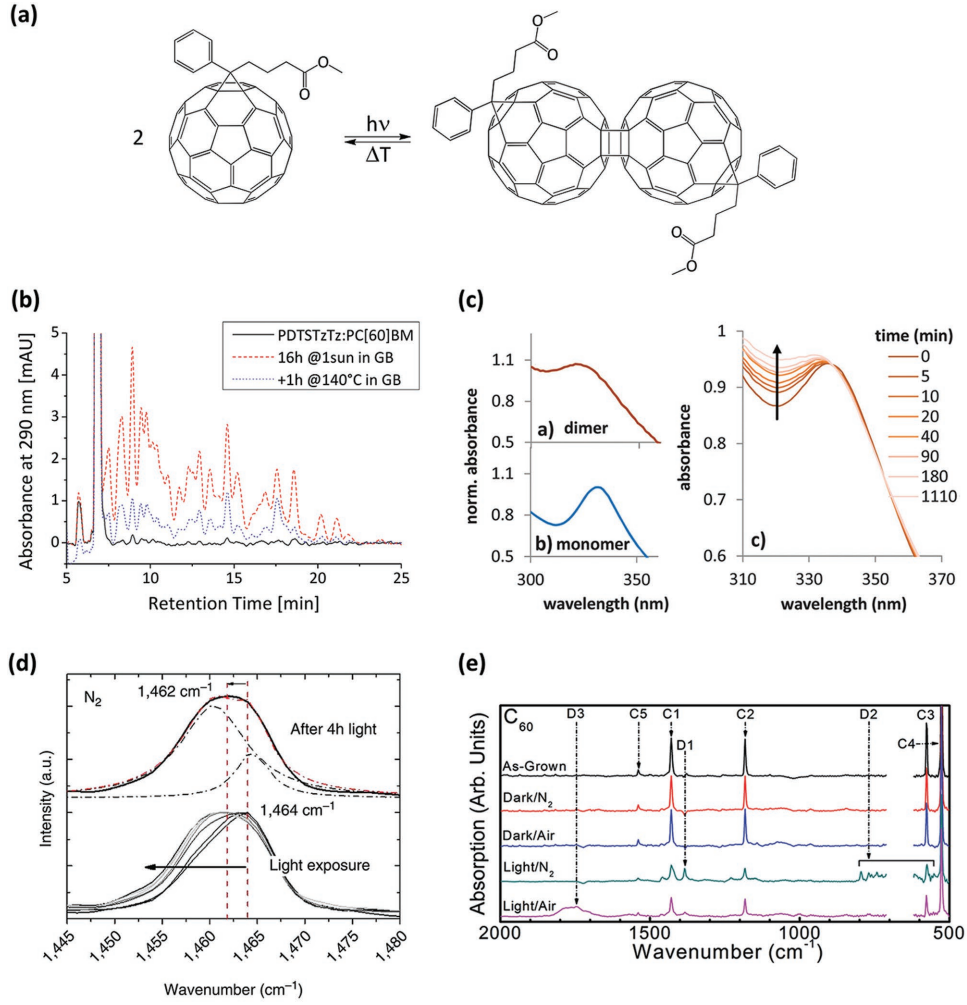

Figure 7. a) Mechanism of $PC_{60}BM$ dimerization, reproduced with permission.[6a] Copyright 2015, A. Distler, and b–e) analytical techniques employed for the identification of dimerization of the fullerene phase. b) HPLC data of fullerene extracts from pristine (poly [(4,4′-bis (2-ethylhexyl) dithieno [3,2-*b*:2′,3′-d] silole)-2,6-diyl-alt-(2,5-bis 3-tetradecylthiophen-2-yl thiazolo 5,4-d thiazole)-2,5diyl]) PDTSTzTz:$PC_{60}BM$ (black line), after illumination (red dashed line), and after subsequent thermal annealing (blue dots). Reproduced with permission.[6b] Copyright 2014, John Wiley & Sons. c) UV/Vis absorption spectra of monomeric $PC_{60}BM$, dimerized $PC_{60}BM$, and spectral changes of a $PC_{60}BM$ film upon illumination. Reproduced with permission.[53a] Copyright 2016, The Royal Society of Chemistry. d) Raman spectroscopic data for neat $PC_{60}BM$ film after 4 hours of exposure to fluorescent light and for pristine $PC_{60}BM$ film upon laser exposure (10–110 s). Reproduced with permission.[91a] Copyright 2013, Macmillan Publishers Ltd. (e) Fourier transform infrared (FTIR) absorption spectra of as-grown C_{60} films and degraded under different conditions. Reproduced with permission.[92] Copyright 2015, The Royal Society of Chemistry.

two separate monomers occurs,[6] which is in line with previous reports on non-substituted and mono-substituted C_{60}.[66,72d] A certain extent of dimerization is reported to occur even when the sample is exposed to small amounts of light (e.g., ambient light in the laboratory),[53a,91a] In fact, the dimerization rate of $PC_{60}BM$ has been identified independent of the energy of the photons absorbed but directly proportional to the light intensity.[6a] In Figure 8b, the increase in absorbance at 320 nm is plotted versus the amount of absorbed photons for $PC_{60}BM$ films irradiated using filters transmitting different wavelengths. The kinetics of the process were the same for all filters, thus indicating that the extent of dimerization is not influenced by the wavelength of the photons but only by the total amount absorbed.

Dimerization also occurs when the fullerene derivative is blended with conjugated polymers,[6,53a,91a,c] while both the dimerization rate and the extent depends on the polymer it is blended to (Figure 8c). More crystalline polymers like P3HT[94] or PDSTsTzTz,[13b] which lead to bigger size domains of both pure polymer and fullerene, displayed higher extents of fullerene dimerization, whereas less-ordered Si-PCPDTBT[17d] and amorphous PCPDTBT[95] showed low to negligible changes upon illumination.[6a,53a] It was proposed that amorphous polymers, which allow an efficient intermixing with the fullerene, decrease the probability for fullerene molecules to be closer to each other and correctly aligned for dimerization.[53a] Furthermore, $PC_{60}BM$ dimerization competes with charge transfer between the polymer and the fullerene, which occurs

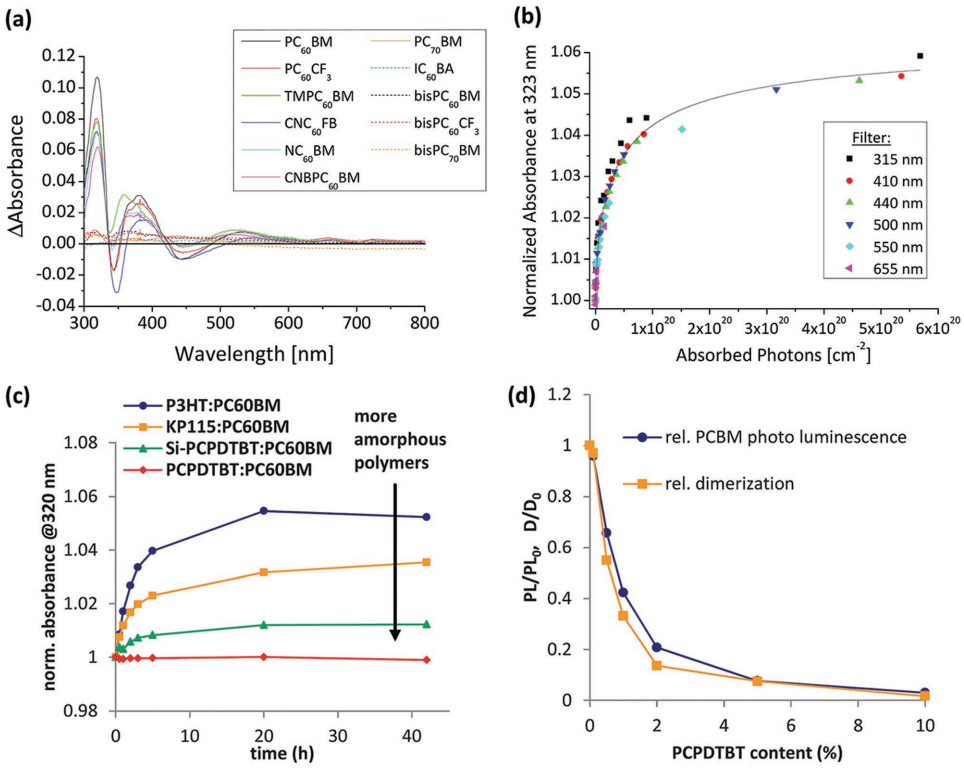

Figure 8. a) Normalized differential absorption spectra of mono- and bis-substituted fullerene derivatives after irradiation in N_2. Reproduced with permission.[6a] Copyright 2015, A. Distler. b) Normalized absorbance versus absorbed photons for PC60BM films irradiated through filters of different cut-offs. Reproduced with permission.[6a] Copyright 2015, A. Distler. c) Left: Normalized absorbance upon irradiation of $PC_{60}BM$ blended with polymers yielding different extents of aggregation. Right: Correlation between PC60BM photoluminescence and extent of dimerization (increase in absorbance at 320 nm) as a function of PCPDTBT content. Panels c) and d) are reproduced with permission.[53a] Copyright 2016, The Royal Society of Chemistry.

more readily in amorphous, well-mixed systems with more polymer:fullerene interfaces available.[6a,53a] Indeed, photoluminescence studies on the amorphous PCPDTBT:$PC_{60}BM$ system indicated coincident trends for the quenching of fullerene photoluminescence and the decrease in the extent of dimerization as PCDTBT content was increased in the samples (see Figure 8d), this giving evidence for a dimerization mechanism driven by excitons on the fullerene phase.[6a,53a] Whilst the general mechanism of photopolymerization of C_{60} and the photodimerization of $PC_{60}BM$ in thin films is proposed as a [2+2] cycloaddition between two parallel [6-6] double bonds on adjacent fullerene cages (see Figure 7a), it is still not fully understood which photoexcited species are involved in the process. However, since the presence of molecular oxygen prevents oligomerization,[72b,73] all mechanistic proposals include fullerene triplet excited states in one way or another. Accordingly, some groups propose a bimolecular reaction between a fullerene in its triplet state and another one in its ground state,[96] some others suggest the reaction between two fullerenes in their triplet states,[72c] and others indicate a step-wise excitation including a dimer intermediate.[97] These mechanistic proposals are all based on the general understanding that triplets are formed in C_{60} films in high yield via intersystem crossing from singlet states, as it was reported for fullerenes in solution.[98] Nevertheless, some groups have indicated no detection of triplet states in $PC_{60}BM$ films using the same measurement techniques (namely, transient absorption spectroscopy),[6a,99] this suggesting that the yield and/or lifetime of fullerene triplet states via intersystem crossing is actually much lower in the solid state compared to that in solution. It was proposed instead that fullerene excitons can rapidly dissociate into cations ($PC_{60}BM^+$) and anions ($PC_{60}BM^-$) in the fullerene phase. After that, these trapped charges can bimolecularly recombine and populate the emissive singlet states and triplet states, the latter able to initiate dimerization.[6a] Additionally, dimerization via charged fullerenes has also been predicted using quantum calculations.[100] A mechanism involving fullerene ions would be in line with recent reports on the dependence of $PC_{60}BM$ dimerization on the V_{oc} of devices.[53a]

Illumination (under N_2) of organic solar cells where the active layer comprises a system favorable to dimerization provokes a decrease in efficiency following a "hockey stick" behavior, also called "burn-in" period, see **Figure 9**a. The efficiency decay is mainly due to the loss of fill factor (FF) and of short circuit current (J_{sc}). Notably, these losses can be eliminated or diminished if the aforementioned factors influencing dimerization are taken into account, for instance using bis-substituted fullerenes (e.g., bis-$PC_{60}BM$),[6] inducing crystallinity in the fullerene phase,[53a] or reducing the crystallinity/domain sizes of the polymer donor.[53a] Concerning the latter, it is noteworthy that measures to prevent dimerization (and increase stability) can be counterproductive for devices, as both polymer crystallinity and suitable domain sizes are necessary to achieve high efficiencies.[101] Additionally, light-induced dimerization has shown

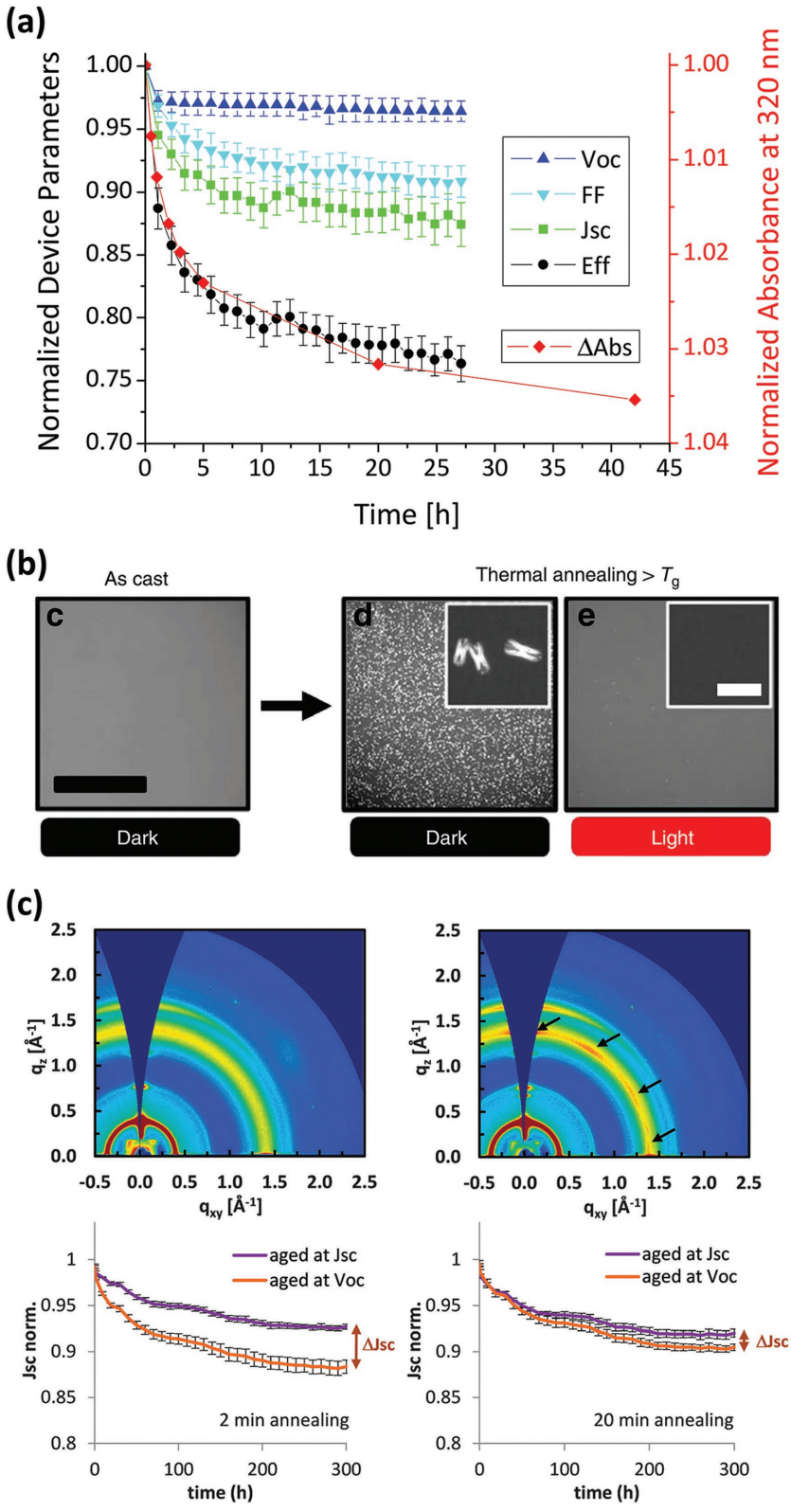

Figure 9. a) Evolution of the electrical parameters of (poly [(4,4′-bis (2-ethylhexyl) dithieno [3,2-b:2′,3′-d] silole)-2,6-diyl-alt-(2,5-bis 3-tetradecylthiophen-2-yl thiazolo 5,4-d thiazole)-2,5diyl]) (PDTSTzTz):$PC_{60}BM$ solar cells and the absorbance at 320 nm of PDTSTzTz:$PC_{60}BM$ films as they are irradiated under inert atmosphere. Reproduced with permission.[6a] Copyright 2015, A. Distler. b) From left to right, optical microscopy images of PCDTBT:PC60BM films as-cast, after thermal annealing at 140 °C for 1 hour, and after thermal annealing preceded by light processing. Reproduced with permission.[91a] Copyright 2013, Macmillan Publishers Ltd. c) Grazing incidence X-ray diffraction (GIXD) pattern of a P3HT:PC60BM films annealed at 140 °C for (left) 2 min and (right) 10 min. J_{sc} evolution for devices annealed for (left) 2 min and (right) 20 min prior to light irradiation held at J_{sc} or V_{oc} conditions. Reproduced with permission.[53a] Copyright 2016, The Royal Society of Chemistry.

a strong dependence on the electrical bias, in such a way that higher amounts of dimers (and higher J_{sc} losses) were detected when devices were aged at V_{oc} (where no charge carriers are extracted) than at J_{sc} conditions (see Figure 9c).[53a] A higher amount of available charges under V_{oc} conditions is presumably the reason behind the enhanced dimer formation; however, if this reaction occurs directly via polarons/charged fullerenes or via excited triplets populated after recombination of charged fullerenes is still uncertain and subject of further investigations. As for the reason behind the J_{sc} losses, literature indicates lower exciton diffusion lengths,[53a,92] exciton dissociation,[53a] and inefficient charge extraction due to lowered electron mobility and creation of traps.[6,53a]

In contrast to the results obtained for light ageing, fullerene dimerization has been revealed beneficial for organic solar cells aged under thermal stress.[91] It is well known that when the active layer is treated at high temperatures, fullerene acceptors like $PC_{60}BM$ can grow to micrometer-sized crystalline domains, reducing the donor–acceptor interface and resulting in severe degradation of device performances.[91b,102] Exemplified in Figure 9b, stabilization of the morphology in the active layer with suppression of fullerene crystals formation can be achieved when modest light exposure (triggering dimerization) precedes thermal annealing, this correlating with higher device stability upon thermal stress.[91a] In this sense, light-processing the active layer represents an easy-to-implement treatment to secure the bulk-heterojunction morphology, which would avoid other morphology-stabilizing strategies such as incorporating additives to the active layer.[103] Probably more relevant to the actual processes occurring in solar cell devices are the studies on simultaneous light and thermal ageing of blends with $PC_{60}BM$,[91c] which also concluded that reduced morphological changes occurred upon thermal annealing under illumination compared to annealing in the dark.[91c]

Since the oligomerization process is reversible at temperatures beyond 100 °C,[72d,104] combined action of light and temperature above this threshold creates a competition between photoinduced dimers formation and dimer depletion via the thermally induced reverse reaction. In line with this, $PC_{60}BM$ segregation was completely prevented when annealing at 85 °C, but light treatment was less effective as temperature increased up to 150 °C.[91c] In contrast, Wong et al. indicated that $PC_{60}BM$ deoligomerization already starts at 85 °C, and follows an Arrhenius temperature dependence with activation energy 0.96 ± 0.04 eV.[91e] The competition between dimer production and the corresponding retro-reaction makes it arduous to relate dimer concentration and morphological control. This aspect was investigated by McCulloch et al. by adding a controlled concentration of synthetically produced, thermally stable fullerene dumbbell $(PCB)_2C_2$.[105] Formation of micrometer-sized $PC_{60}BM$ crystallites was completely prevented upon addition 20% of this dimer, although lower loads were also observed to suppress, to different extents, crystal formation. A modest increase in device performances was also observed up to such loading, starting from which PCE decreased due to lower J_{sc} values. This decrease correlated with lower electron mobilities determined by measurements in OFETs[105] and in line with results obtained for light-induced degradation of solar cells.[6,53a] These results also help to explain why light-processing prior to thermal annealing appears to be non-detrimental for solar cell performances compared to light degradation experiments. Whilst both approaches induce $PC_{60}BM$ oligomerisation, the fact that low irradiation doses are used in thermal experiments (e.g., < 10 mW cm^{-2})[105] compared to light-soaking experiments (1000 mW cm^{-2})[6] leads to largely different dimer concentrations in the blend, thus provoking different effects in UV/Vis absorption, photoluminescence or solar cell performances.[6,53a,91a,e] Interestingly, $PC_{60}BM$ nucleation has been prevented via light-processing in blends with a wide range of polymers, both amorphous and crystalline,[91a,c,e] which contrasts with the results of Heumueller et al. indicating lower/negligible dimerization for more amorphous polymers.[53a] This finding suggests that very low dimer quantities are able to prevent nucleation upon thermal stress, at a stage where no effects on UV/Vis absorption and device performance can be observed yet.

Fullerenes and Morphological Stabilization of the Active Layer: Stabilizing bulk-heterojunction morphology is possible through alternative procedures, which often require the functionalization of the fullerene acceptor or its incorporation into sophisticated polymer structures. For instance, the fullerene cage can be functionalized with bulky substituents like triphenylamine (TPA) or 9,9-dimethylfluorene (MF) (see **Figure 10**a) to obtain amorphous fullerene acceptors able to prevent phase segregation in the active layer.[106] A stabilizing strategy commonly referred in the literature is the crosslinking of the active layer components, either establishing donor-donor, donor–acceptor or acceptor-acceptor links.[107] To this end, donor and/or acceptor are furnished with chemical functionalities whose reactivity can be triggered by heat or light once the active layer has been processed to a suitable morphology. Crosslinking between donor and acceptor is frequently achieved via functionalization of the polymer donor.[107,108] For instance, Gholamkass et al. reported the use of an azide-functionalized graft copolymer of P3HT able to selectively add to the fullerene cage via a thermally induced cycloaddition reaction (see Figure 10c).[108b] This approach allowed the prevention of crystal growth upon thermal ageing, together with a modest reduction of the device degradation rate compared to control samples (33% versus 20% PCE retention after 5 h at 150 °C).[108b] This same chemistry was explored by Derue et al. with the use of the bis-azide crosslinker 4,4-bis(azidomethyl)-1,1-biphenyl (BABP), able to stabilize the morphology in different polymer:fullerene combinations by selective binding to $PC_{60}BM$ or $PC_{70}BM$.[109] Additionally, fullerenes have been modified with acetylenic, styryl, epoxide, oxetane and silyl groups to crosslink the active layer establishing acceptor-acceptor bonds.[107a,110] This strategy is exemplified in Figure 10b by the work of Cheng et al., who produced styryl-functionalized fullerene derivatives that undergo in situ polymerization when treated thermally.[110a] Incorporation of these functionalized fullerenes as additives allowed preserving the active layer morphology and device performances over time (3.7% average PCE upon thermal annealing at 150 °C for 25 h).[110a] Alternatively, fullerenes can be incorporated into a wide range of polymer structures (e.g., side-chain or main-chain polyfullerenes, double cable structures) and then used as acceptors or additives in the active layer.[111] As an example, novel main chain polyfullerenes have been recently synthesized using sterically controlled azomethine ylide cycloaddition polymerization (see Figure 10d for chemical structure).[111a] A detailed insight about the different types of polyfullerenes and their incorporation to solar cells is, however, beyond the scope of this work, and the reader is directed to comprehensive publications on the subject.[111f] Even so, it is noteworthy mentioning fullerene-containing block copolymers as an interesting approach to create morphologies that are preserved over time.[111] Block copolymers consist of alternating segments or blocks, whose inherent immiscibility leads to a self-assembling process called "microphase separation", particularly relevant for their application in organic photovoltaics.[112] On the one hand, the domain sizes are created on the nanometer length scale, which is coincident with the exciton-diffusion length scale in organic semiconductors. On the other hand, the created nanostructures are thermodynamically favored, which confers to them long term stability.[111h,i] Accordingly, block copolymers consisting of chemically bonded donor–acceptor segments can be used as single components of the active layer yielding enhanced thermal stability.[111h] However, such morphological stabilization is frequently attained in detriment of the device performance, which is affected by unbalanced charge carrier mobilities in the donor and acceptor blocks. In this regard, Hufnagel et al. have recently described that charge carrier mobility mismatch in the diblock copolymer P3HT-*b*-$PPC_{60}BM$ (where $PPC_{60}BM$ indicates a polystyrene copolymer with pendant fullerenes, depicted in Figure 10e) could be solvented by blending it with additional $PC_{60}BM$ loading. This strategy was able to balance the hole/electron mobilities, bringing them to values comparable to those in P3HT:$PC_{60}BM$ blends whilst retaining the positive effects of the block copolymer over morphological stability.[111b] Fullerene-containing block copolymers such as the one shown in Figure 10 can also be used as compatibilizers in conventional polymer-fullerene blends, reducing

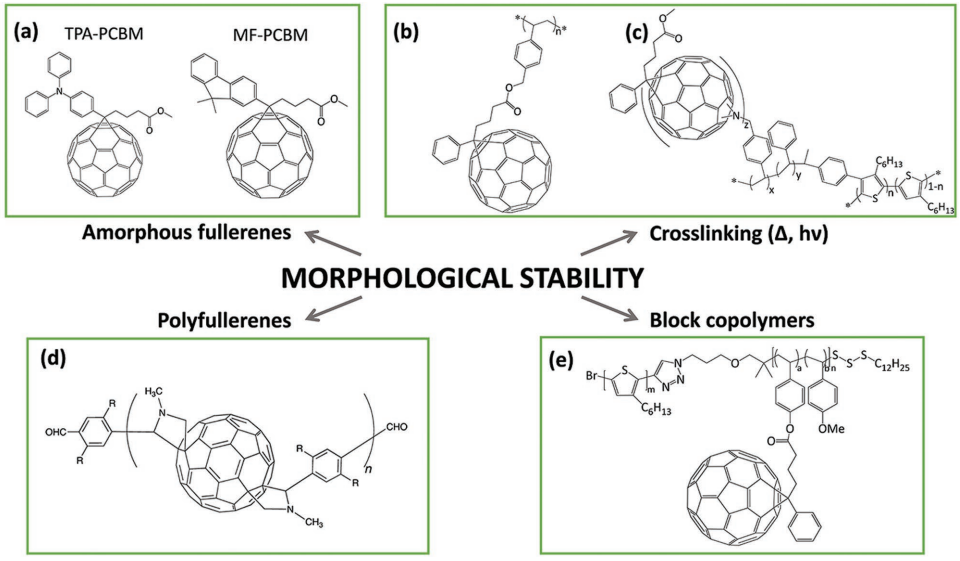

Figure 10. Strategies to improve bulk-heterojunction morphology. a) Amorphous fullerene derivatives for better morphological control.[106a] b) In situ polymerizable styrene-functionalized $PC_{60}BM$ designed by Cheng et al.[110a] c) Thermally induced cycloaddition between an azide functionalized P3HT copolymer and the fullerene cage.[108b] d) Novel main chain polyfullerenes synthesized via the metal-free SACAP route.[111a] e) Diblock copolymer consisting of a P3HT donor segment and a polystyrene copolymer with pendant $PC_{60}BM$ as acceptor.[111b]

the interfacial energy between P3HT and $PC_{60}BM$ and preventing phase separation.[113] Finally, control over fullerene crystallization does not always require complex synthetic procedures or processing treatments.[114] Different groups have reported the benefits of using fullerene mixtures like $PC_{60}BM$:$PC_{70}BM$,[114b,e,110b,e] $PC_{60}BM$:bis-$PC_{60}BM$,[114a,c,110a,c] $IC_{60}BA$:$PC_{70}BM$,[114f] or $PC_{60}BM$:C_{60},[114d,110d] instead of single-fullerenes as acceptors in the active layer. This stabilizing "alloy acceptor" approach, which has often also positive effects over device performance,[114c,e,115,110c,e,111] can additionally reduce the costs of the acceptor material if the employed mixture combines fullerenes obtained as main and by-products of the same synthetic route.[114b,g]

5. Other Carbon Materials: Carbon Nanotubes

5.1. Properties

Fullerene derivatives remain the most widely employed carbon materials used in the active layer of organic solar cells.[61] Although less extensively used, other nanostructured allotropic forms of carbon have received considerable attention for their use as active materials, particularly carbon nanotubes (CNTs).[116] Carbon nanotubes consist of single layers of sp^2 carbon rolled up into cylindrical nanostructures. They can be classified as single-walled (SWCNTs) or multi-walled (MWCNTs) depending on if they consist of single or multiple concentric tubes, respectively. The optical and electronic properties of carbon nanotubes are determined by (and can be tuned by) their physical structure, which is defined by the rolling angle (characterized by the chiral indices n and m) and diameter of the cylinders. Accordingly, carbon nanotubes can be either metallic or semiconductors, and offer selective or broadband absorption of light from the near infrared to the ultraviolet region.[116d,117] Their properties can be also further tuned by doping[118] or by coupling nanotubes into bundles.[119]

Carbon nanotubes combine lightweight and high aspect ratio with exceptional mechanical properties,[120] being one of the strongest materials known, yet displaying very high flexibility upon bending.[121] Although generally inert, the curvature of the CNTs enhances their chemical reactivity compared to flat graphene.[122] In turn, this allows the functionalization of the carbon nanotubes, which can be certainly useful to debundle CNTs in order to facilitate their processing in solution or their incorporation into polymer matrices.[116a,c] Concerning their thermal stability, carbon nanotubes are reported to be more stable to oxidation than other forms of carbon (such as amorphous or activated carbon),[116c] and have been indicated to act as polymer antioxidants under these conditions.[123] However, the photochemistry of CNTs is still not fully understood. According to the literature, irradiation in presence of oxygen of these carbon species can lead to both the generation and the consumption of radical oxygen species, this depending on the characteristics of nanotubes, their functionalization, and the reaction conditions.[124] In line with this, polymer:CNTs composites have been shown to display both enhanced and reduced photodegradation rates compared to pristine polymers, often depending on the CNTs loading.[121,125] Thus, further studies about the photochemistry of CNTs remain essential to understand the implications that CNTs can have towards solar cell stability.

5.2. CNTs and Organic Solar Cells Stability

The application of carbon nanotubes in organic photovoltaics is determined by their optoelectronical properties. In general terms, whilst metallic or doped carbon nanotubes can be used as electrodes because of high conductivity and their mechanical

flexibility, semiconducting species are interesting materials for the active layer, either able to enhance charge separation and collection or act as light absorbers.[118a,119,126] Although reports assessing the effect of CNTs in OSCs stability are scarce to date, some promising results have been obtained for the enhancement of solar cell stability. For instance, Rowell et al. have explored flexible characteristics of SWCNTs to replace ITO as transparent electrode. In their study, simple bending tests performed identically for the two variations led to 20–25% PCE losses in PET/SWCNTs solar cells (initial PCE = 2.5–1.2%) and total failure and visible fractures for PET/ITO devices (initial PCE = 3%).[127] Additionally, annealing of SWCNTs devices after the bending test led to the recovery of the initial efficiencies. Carbon nanotubes have been also shown beneficial for the overall stability to light of organic solar cells. Dembele et al. observed enhanced power conversion efficiencies (4.1% versus 3.7%) and retained efficiencies upon light soaking in dye-sensitized solar cells using TiO_2-MWCNTs composites as anodes compared to cells using pure TiO_2 layers.[128] The authors proposed that the enhanced photostability could be due to the formation of MWCNTs conducting networks able to limit charge recombination, although they did not exclude possible effects due to the interaction between the anode and the photoactive dye. Remarkably, enhanced photostability has been observed for P3HT composites with MWCNTs exposed to light in chloroform solution,[129] as well as for P3HT:PC_{60}BM blends with MWCTNs, both in films and in solution.[130] Ratha et al. observed a maximum stabilization to photooxidation for composites in concentration P3HT:PC_{60}BM (7%) – MWCNTs (3%), whilst higher and lower loads of MWCNTs led to enhanced degradation rates (similar to pristine P3HT:PC_{60}BM composites).[130a] As for the reason behind the photostabilities of the different composites, the authors indicated a trade-off between the stabilizing effect brought by CNTs as they coat the P3HT surface and the destabilization provoked by metal impurities present in the MWCNTs sample. Concerning their effect on devices, Singh et al. recently studied the stability of cells where the P3HT:PC_{60}BM active layer was doped with MWCNTs amounts ranging from 0.1% to 0.3%.[130b] Optimized devices (0.2% MWCNTs load) displayed enhanced performance (2.71% versus 1.33% in the control device) together with improved stability when kept under vacuum or at ambient atmosphere for a period of 288 hours (samples were exposed to light only during *J–V* characterization). The optical properties of active layer films remained virtually unchanged when kept under the same conditions, whereas changes in hole and electron mobility could be observed, particularly for samples kept in air. Accordingly, the decrease in device performance over time was ascribed to the creation of trapping sites and recombination centers.

Overall, the incorporation of carbon nanotubes into OSCs presents limitations related to the inhomogeneity of the CNTs samples and their processing requirements.[116c] Additionally, many articles fail to report a complete characterization of the nanotubes being employed in their studies. As an example, after the synthesis and purification of SWCNTs, samples contain a mixture of both semiconducting and metallic tubes, which have antagonist effects towards solar cell operation (and presumably, stability) if processed in the photoactive layer.[116c] This makes the use of carbon nanotubes in organic solar cells profoundly influenced by the developments towards the selective isolation of the wide variety of nanotube species (in terms of electronic properties, diameter, length, or quirality) with high purity and in appropriate yields. Advances in synthesis, purification, and processing of CNTs,[131] together with a deep understanding of the photophysical and photochemical properties of these materials,[116d] are key elements to eventually allow the exploitation of CNTs in organic solar cells with enhanced operational lifetimes.

6. Conclusions

In this progress report, we have described the recent progress in understanding the influence of nanostructured carbon materials on the stability of OSCs. A growing body of detailed knowledge becomes available, enabling targeted approaches to exploit and maximize the stabilizing effects that these materials can have over the degradation of the active layer, and, as a consequence, over the performance of the resulting devices.

Donor polymers are degraded upon exposure to oxygen and light. Already low levels of photooxidation cause a large detrimental effect on the electrical performance of OSCs. The standard-absorber P3HT has been found to predominantly degrade via a radical-based photooxidation mechanism that proceeds at high rates especially if irradiated in the UV spectral region. Here, the acceptor material PC_{60}BM can stabilize the donor material by a variety of mechanisms, like the inner filter effect, exerted by the strong UV absorption of PC_{60}BM. The strongest stabilization effect comes however from the action of PC_{60}BM as non-sacrificial radical scavenging agent. Thus, maximizing these stabilization effects of PC_{60}BM on the donor polymer can be used as a tool to achieve longer operational lifetimes even using cheaper encapsulation materials.

Additionally, fullerene derivatives are involved in degradation phenomena that do not include atmospheric oxygen and thus occur even under complete oxygen exclusion. The so-called "burn-in" phenomenon, an initial rapid performance loss, has been shown to derive from PC_{60}BM dimerization proceeding via a photochemically allowed, thermally reversible 2 + 2 cycloaddition. Analysis of the parameters influencing the dimerization rate and the equilibrium position has shown, among others, a dependency on the fullerene molecular structure (reduced in C70-based and bis-substituted fullerene derivatives), its crystallinity, and the molecular packing of the donor polymer. Importantly, fullerene dimers can have a positive influence on OSCs stability as they preserve the morphology of the bulk heterojunction upon thermal stress. Low-level irradiation during processing (to induce a small amount of PC_{60}BM dimers that hinder the free movement of the PC_{60}BM phase towards crystal growth) can be exploited as a simple method to improve thermal stability of OSCs. However, the aforementioned factors influencing fullerene oligomerization should be also taken into account as for preventing the higher amounts of dimers, which, in turn, negatively influence the performance of the devices.

Another smart and cost-efficient approach for morphological stabilization is the use of fullerene mixtures as acceptors, which often consist of a main product and a byproduct of a

certain synthetic route. This way, higher thermal stability can be achieved without penalizing performance and production costs. Overall, morphology-stabilizing strategies should aim at creating thermodynamically stable nanostructures that are also beneficial for yielding high performance solar cells. To this end, additives and compatibilizers can be used to reduce the surface energy (to minimize the tendency for crystal growth) so that the entropy contribution keeps the crystallites small. Another approach is the use of fullerene-containing block copolymers, which undergo microphase separation to create domains in the nanometer length scale. Such nanostructures can be favorable for the operation the device, while remaining the thermodynamic minimum preferred for long-term stability.

In sum, research conducted to increase the performance of OSCs has led to very promising results over the past years, currently yielding power conversion efficiencies that can be competitive on the market. However, the industrial commercialization and establishment of this photovoltaic technology into the market requires a correct balance among efficiency, stability and cost. Fullerene derivatives, widely employed as acceptor materials, often meet also the requirement of achieving high and consistent efficiencies when blended with adequate polymer donors. Additionally, as discussed throughout this review, fullerenes possess interesting stabilizing properties, which can be exploited and tuned to create active layers presenting an enhanced stability against photo- and thermally induced processes. Since the fabrication of devices with higher intrinsic stabilities can, in turn, reduce costs derived from the encapsulation of the modules, the use of fullerene derivatives is a promising approach to fulfill the three main requirements to OSCs commercialization. In addition to this, the freedom of design and integration of OSCs are unique selling points that open a new market other photovoltaic technologies cannot address.

Acknowledgments

This work has been funded by the EC (ITNs "ESTABLIS" and "POCAONTAS", project Nos 290022 and 316633, respectively, and the COFUND program AMAROUT), by the Autonomouus Community of Madrid (Project "FotoCarbon", S2013/MIT-2841) and by the Spanish Ministry of Economy and Competitiveness (Project MultiCrom, CTQ2014-58801).

Received: June 18, 2016
Revised: July 30, 2016
Published online:

[1] C. J. M. Emmott, J. A. Rohr, M. Campoy-Quiles, T. Kirchartz, A. Urbina, N. J. Ekins-Daukes, J. Nelson, *Energy Environ. Sci.* **2015**, *8*, 1317.

[2] Heliatek in http://www.heliatek.com/en/press/press-releases/details/heliatec-sets-new-organic-photovoltaic-world-record-efficiency-of-13-2, accessed: June, 2016.

[3] a) R. Steim, T. Ameri, P. Schilinsky, C. Waldauf, G. Dennler, M. Scharber, C. J. Brabec, *Solar Energy Mater. Solar Cells* **2011**, *95*, 3256; b) K. Rühle, M. K. Juhl, M. D. Abbott, M. Kasemann, *IEEE J. Photovolt.* **2015**, *5*, 926.

[4] a) N. Grossiord, J. M. Kroon, R. Andriessen, P. W. M. Blom, *Org. Electron.* **2012**, *13*, 432; b) M. Jørgensen, K. Norrman, F. C. Krebs, *Solar Energy Mater. Solar Cells* **2008**, *92*, 686; c) M. Jørgensen, K. Norrman, S. A. Gevorgyan, T. Tromholt, B. Andreasen, F. C. Krebs, *Adv. Mater.* **2012**, *24*, 580; d) P. Cheng, X. Zhan, *Chem. Soc. Rev.* **2016**, *45*, 2544.

[5] G. Yu, J. Gao, J. C. Hummelen, F. Wudl, A. J. Heeger, *Science* **1995**, *270*, 1789.

[6] a) A. Distler, in *The Role of Fullerenes in the Photo-Degradation of Organic Solar Cells*, Vol. Friedrich-Alexander-Universität Erlangen-Nürnberg (FAU), **2015**; b) A. Distler, T. Sauermann, H.-J. Egelhaaf, S. Rodman, D. Waller, K.-S. Cheon, M. Lee, D. M. Guldi, *Adv. Energy Mater.* **2014**, *4*, 1.

[7] a) I. Fraga Domínguez, P. D. Topham, P.-O. Bussière, D. Bégué, A. Rivaton, *J. Phys. Chem. C* **2015**, *119*, 2166; b) M. Manceau, A. Rivaton, J.-L. Gardette, S. Guillerez, N. Lemaître, *Polym. Degrad. Stab.* **2009**, *94*, 898; c) M. Manceau, J. Gaume, A. Rivaton, J.-L. Gardette, G. Monier, L. Bideux, *Thin Solid Films* **2010**, *518*, 7113; d) A. Tournebize, P.-O. Bussière, P. Wong-Wah-Chung, S. Thérias, A. Rivaton, J.-L. Gardette, S. Beaupré, M. Leclerc, *Adv. Energy Mater.* **2013**, *3*, 478; e) A. Rivaton, A. Tournebize, J. Gaume, P.-O. Bussière, J.-L. Gardette, S. Therias, *Polym. Int.* **2014**, *63*, 1335.

[8] a) A. Distler, P. Kutka, T. Sauermann, H.-J. Egelhaaf, D. M. Guldi, D. Di Nuzzo, S. C. J. Meskers, R. A. J. Janssen, *Chem. Mater.* **2012**, *24*, 4397; b) E. T. Hoke, I. T. Sachs-Quintana, M. T. Lloyd, I. Kauvar, W. R. Mateker, A. M. Nardes, C. H. Peters, N. Kopidakis, M. D. McGehee, *Adv. Energy Mater.* **2012**, *2*, 1351; c) M. Manceau, E. Bundgaard, J. E. Carle, O. Hagemann, M. Helgesen, R. Sondergaard, M. Jorgensen, F. C. Krebs, *J. Mater. Chem.* **2011**, *21*, 4132; d) M. Manceau, M. Helgesen, F. C. Krebs, *Polym. Degrad. Stab.* **2010**, *95*, 2666.

[9] a) S. Chambon, A. Rivaton, J.-L. Gardette, M. Firon, L. Lutsen, *J. Polym. Sci. Part A: Polym. Chem.* **2007**, *45*, 317; b) P.-O. Bussière, A. Rivaton, S. Thérias, J.-L. Gardette, *J. Phys. Chem. B* **2011**, *116*, 802; c) H. Hintz, H. J. Egelhaaf, H. Peisert, T. Chassé, *Polym. Degrad. Stab.* **2010**, *95*, 818; d) H. Hintz, C. Sessler, H. Peisert, H J. Egelhaaf, T. Chassé, *Chem. Mater.* **2012**, *24*, 2739.

[10] J. Ahmad, K. Bazaka, L. J. Anderson, R. D. White, M. V. Jacob, *Renew. Sustain. Energy Rev.* **2013**, *27*, 104.

[11] a) G. Dennler, M. C. Scharber, C. J. Brabec, *Adv. Mater.* **2009**, *21*, 1323; b) N. C. Giebink, G. P. Wiederrecht, M. R. Wasielewski, S. R. Forrest, *Phys. Rev. B* **2011**, *83*, 195326; c) U. Wurfel, D. Neher, A. Spies, S. Albrecht, *Nat. Commun.* **2015**, *6*, 6951.

[12] C. H. Peters, I. T. Sachs-Quintana, W. R. Mateker, T. Heumueller, J. Rivnay, R. Noriega, Z. M. Beiley, E. T. Hoke, A. Salleo, M. D. McGehee, *Adv. Mater.* **2012**, *24*, 663.

[13] a) J. P. Bastos, E. Voroshazi, E. Fron, G. Brammertz, T. Vangerven, M. Van der Auweraer, J. Poortmans, D. Cheyns, *ACS Appl. Mater. Interfaces* **2016**, *8*, 9798; b) T. Heumueller, W. R. Mateker, I. T. Sachs-Quintana, K. Vandewal, J. A. Bartelt, T. M. Burke, T. Ameri, C. J. Brabec, M. D. McGehee, *Energy Environ. Sci.* **2014**, *7*, 2974.

[14] a) G. E. Morse, A. Tournebize, A. Rivaton, T. Chasse, C. Taviot-Gueho, N. Blouin, O. R. Lozman, S. Tierney, *Phys. Chem. Chem. Phys.* **2015**, *17*, 11884; b) S. Karuthedath, T. Sauermann, H.-J. Egelhaaf, R. Wannemacher, C. J. Brabec, L. Luer, *J. Mater. Chem. A* **2015**, *3*, 3399.

[15] F. Deschler, A. De Sio, E. von Hauff, P. Kutka, T. Sauermann, H.-J. Egelhaaf, J. Hauch, E. Da Como, *Adv. Funct. Mater.* **2012**, *22*, 1461.

[16] M. Campoy-Quiles, T. Ferenczi, T. Agostinelli, P. G. Etchegoin, Y. Kim, T. D. Anthopoulos, P. N. Stavrinou, D. D. C. Bradley, J. Nelson, *Nat. Mater.* **2008**, *7*, 158.

[17] a) L. Lüer, H. J. Egelhaaf, D. Oelkrug, G. Cerullo, G. Lanzani, B. H. Huisman, D. de Leeuw, *Org. Electron.* **2004**, *5*, 83; b) J. Guo, H. Ohkita, H. Benten, S. Ito, *J. Am. Chem. Soc.* **2010**, *132*, 6154;

c) J. Peet, L. Wen, P. Byrne, S. Rodman, K. Forberich, Y. Shao, N. Drolet, R. Gaudiana, G. Dennler, D. Waller, *Appl. Phys. Lett.* **2011**, *98*, 043301; d) M. Morana, H. Azimi, G. Dennler, H.-J. Egelhaaf, M. Scharber, K. Forberich, J. Hauch, R. Gaudiana, D. Waller, Z. Zhu, K. Hingerl, S. S. van Bavel, J. Loos, C. J. Brabec, *Adv. Funct. Mater.* **2010**, *20*, 1180.

[18] B. Movaghar, M. Grünewald, B. Ries, H. Bassler, D. Würtz, *Phys. Rev. B* **1986**, *33*, 5545.

[19] C. J. Brabec, G. Zerza, G. Cerullo, S. De Silvestri, S. Luzzati, J. C. Hummelen, S. Sariciftci, *Chem. Phys. Lett.* **2001**, *340*, 232.

[20] I. A. Howard, R. Mauer, M. Meister, F. Laquai, *J. Am. Chem. Soc.* **2010**, *132*, 14866.

[21] G. Grancini, M. Maiuri, D. Fazzi, A. Petrozza, H. J. Egelhaaf, D. Brida, G. Cerullo, G. Lanzani, *Nat. Mater.* **2013**, *12*, 29.

[22] a) J. Lee, K. Vandewal, S. R. Yost, M. E. Bahlke, L. Goris, M. A. Baldo, J. V. Manca, T. V. Voorhis, *J. Am. Chem. Soc.* **2010**, *132*, 11878; b) K. Vandewal, S. Albrecht, E. T. Hoke, K. R. Graham, J. Widmer, J. D. Douglas, M. Schubert, W. R. Mateker, J. T. Bloking, G. F. Burkhard, A. Sellinger, J. M. J. Fréchet, A. Amassian, M. K. Riede, M. D. McGehee, D. Neher, A. Salleo, *Nat. Mater.* **2014**, *13*, 63.

[23] A. A. Bakulin, A. Rao, V. G. Pavelyev, P. H. M. van Loosdrecht, M. S. Pshenichnikov, D. Niedzialek, J. Cornil, D. Beljonne, R. H. Friend, *Science* **2012**, *335*, 1340.

[24] H. Kraus, M. C. Heiber, S. Väth, J. Kern, C. Deibel, A. Sperlich, V. Dyakonov, *Sci. Rep.* **2016**, *6*, 29158.

[25] J. Noolandi, K. M. Hong, *Phys. Rev. Lett.* **1978**, *41*, 46.

[26] C. Tanase, P. W. M. Blom, D. M. de Leeuw, E. J. Meijer, *Phys. Status Solidi (a)* **2004**, *201*, 1236.

[27] F. Deledalle, P. Shakya Tuladhar, J. Nelson, J. R. Durrant, T. Kirchartz, *J. Phys. Chem. C* **2014**, *118*, 8837.

[28] a) A. Foertig, A. Baumann, D. Rauh, V. Dyakonov, C. Deibel, *Appl. Phys. Lett.* **2009**, *95*, 052104; b) T. Kirchartz, J. Nelson, *Phys. Rev. B* **2012**, *86*, 165201.

[29] A. Seemann, T. Sauermann, C. Lungenschmied, O. Armbruster, S. Bauer, H. J. Egelhaaf, J. Hauch, *Solar Energy* **2011**, *85*, 1238.

[30] a) V. Brand, K. Levi, M. D. McGehee, R. H. Dauskardt, *Solar Energy Mater. Solar Cells* **2012**, *103*, 80; b) V. Brand, C. Bruner, R. H. Dauskardt, *Solar Energy Mater. Solar Cells* **2012**, *99*, 182; c) S. R. Dupont, M. Oliver, F. C. Krebs, R. H. Dauskardt, *Solar Energy Mater. Solar Cells* **2012**, *97*, 171.

[31] A. Wagenpfahl, D. Rauh, M. Binder, C. Deibel, V. Dyakonov, *Phys. Rev. B* **2010**, *82*, 115306.

[32] S. D. Dimitrov, S. Wheeler, D. Niedzialek, B. C. Schroeder, H. Utzat, J. M. Frost, J. Yao, A. Gillett, P. S. Tuladhar, I. McCulloch, J. Nelson, J. R. Durrant, *Nat. Commun.* **2015**, *6*.

[33] J. R. Ochsmann, D. Chandran, D. W. Gehrig, H. Anwar, P. K. Madathil, K.-S. Lee, F. Laquai, *Macromol. Rapid Commun.* **2015**, *36*, 1122.

[34] M. Koppe, H.-J. Egelhaaf, E. Clodic, M. Morana, L. Lüer, A. Troeger, V. Sgobba, D. M. Guldi, T. Ameri, C. J. Brabec, *Adv. Energy Mater.* **2013**, *3*, 949.

[35] I. Fraga Domínguez, in *Identification of the Degradation Mechanisms of Organic Solar Cells: Active Layer and Interfacial Layers*, PhD Thesis, Université Blaise Pascale & Aston University, **2015**.

[36] C. Waldauf, M. C. Scharber, P. Schilinsky, J. A. Hauch, C. J. Brabec, *J. Appl. Phys.* **2006**, *99*, 104503.

[37] a) A. Foertig, J. Rauh, V. Dyakonov, C. Deibel, *Phys. Rev. B* **2012**, *86*, 115302; b) A. Foertig, J. Kniepert, M. Gluecker, T. Brenner, V. Dyakonov, D. Neher, C. Deibel, *Adv. Funct. Mater.* **2014**, *24*, 1306.

[38] a) I. H. M. van Stokkum, D. S. Larsen, R. van Grondelle, *Biochim. Biophys. Acta (BBA)* **2004**, *1657*, 82; b) S. Gélinas, O. Paré-Labrosse, C.-N. Brosseau, S. Albert-Seifried, C. R. McNeill, K. R. Kirov, I. A. Howard, R. Leonelli, R. H. Friend, C. Silva, *J. Phys. Chem. C* **2011**, *115*, 7114.

[39] P. J. Brown, H. Sirringhaus, M. Harrison, M. Shkunov, R. H. Friend, *Phys. Rev. B* **2001**, *63*, 125204.

[40] S. Karuthedath in *Tracing Degradation Effects in Organic Solar Cells*, PhD Thesis, Universidad Autónoma de Madrid, **2015**.

[41] C. G. Shuttle, B. O'Regan, A. M. Ballantyne, J. Nelson, D. D. C. Bradley, J. R. Durrant, *Phys. Rev. B* **2008**, *78*, 113201.

[42] L. Luer, S. Hoseinkhani, D. Polli, J. Crochet, T. Hertel, G. Lanzani, *Nat. Phys.* **2009**, *5*, 54.

[43] R. Rosch, D. M. Tanenbaum, M. Jorgensen, M. Seeland, M. Barenklau, M. Hermenau, E. Voroshazi, M. T. Lloyd, Y. Galagan, B. Zimmermann, U. Wurfel, M. Hosel, H. F. Dam, S. A. Gevorgyan, S. Kudret, W. Maes, L. Lutsen, D. Vanderzande, R. Andriessen, G. Teran-Escobar, M. Lira-Cantu, A. Rivaton, G. Y. Uzunoglu, D. Germack, B. Andreasen, M. V. Madsen, K. Norrman, H. Hoppe, F. C. Krebs, *Energy Environ. Sci.* **2012**, *5*, 6521.

[44] J. W. Kiel, B. J. Kirby, C. F. Majkrzak, B. B. Maranville, M. E. Mackay, *Soft Matter* **2010**, *6*, 641.

[45] a) M. A. Ruderer, P. Muller-Buschbaum, *Soft Matter* **2011**, *7*, 5482; b) P. Müller-Buschbaum, *Adv. Mater.* **2014**, *26*, 7692.

[46] M. S. A. Abdou, F. P. Orfino, Y. Son, S. Holdcroft, *J. Am. Chem. Soc.* **1997**, *119*, 4518.

[47] H. Hintz, H. J. Egelhaaf, L. Lüer, J. Hauch, H. Peisert, T. Chassé, *Chem. Mater.* **2010**, *23*, 145.

[48] a) M. S. A. Abdou, S. Holdcroft, *Macromolecules* **1993**, *26*, 2954; b) Y. W. Soon, H. Cho, J. Low, H. Bronstein, I. McCulloch, J. R. Durrant, *Chem. Commun.* **2013**, *49*, 1291; c) S. Holdcroft, *Macromolecules* **1991**, *24*, 4834.

[49] M. Manceau, A. Rivaton, J.-L. Gardette, *Macromol. Rapid Commun.* **2008**, *29*, 1823.

[50] C. Brabec, C. Waldauf, in *Photovoltaic Component and Production Method Therefor*, US20060141662 A1, United States **2006**.

[51] a) E. Stratakis, M. M. Stylianakis, E. Koudoumas, E. Kymakis, *Nanoscale* **2013**, *5*, 4144; b) W. R. Mateker, I. T. Sachs-Quintana, G. F. Burkhard, R. Cheacharoen, M. D. McGehee, *Chem. Mater.* **2015**, *27*, 404.

[52] I. Topolniak, J.-L. Gardette, S. Therias, *Polym. Degrad. Stabil.* **2015**, *121*, 137.

[53] a) T. Heumueller, W. R. Mateker, A. Distler, U. F. Fritze, R. Cheacharoen, W. H. Nguyen, M. Biele, M. Salvador, M. von Delius, H.-J. Egelhaaf, M. D. McGehee, C. J. Brabec, *Energy Environ. Sci.* **2016**, *9*, 247; b) C. H. Peters, I. T. Sachs-Quintana, J. P. Kastrop, S. Beaupré, M. Leclerc, M. D. McGehee, *Adv. Energy Mater.* **2011**, *1*, 491; c) T. M. Clarke, C. Lungenschmied, J. Peet, N. Drolet, K. Sunahara, A. Furube, A. J. Mozer, *Adv. Energy Mater.* **2013**, *3*, 1473.

[54] a) A. Tournebize, A. Rivaton, J.-L. Gardette, C. Lombard, B. Pépin-Donat, S. Beaupré, M. Leclerc, *Adv. Energy Mater.* **2014**, 1301530; b) S. Chambon, A. Rivaton, J.-L. Gardette, M. Firon, *Solar Energy Mater. Solar Cells* **2008**, *92*, 785.

[55] D. K. Susarova, N. P. Piven, A. V. Akkuratov, L. A. Frolova, M. S. Polinskaya, S. A. Ponomarenko, S. D. Babenko, P. A. Troshin, *Chem. Commun.* **2015**, *51*, 2239.

[56] L. A. Frolova, N. P. Piven, D. K. Susarova, A. V. Akkuratov, S. D. Babenko, P. A. Troshin, *Chem. Commun.* **2015**, *51*, 2242.

[57] M. C. Heiber, C. Baumbach, V. Dyakonov, C. Deibel, *Phys. Rev. Lett.* **2015**, *114*, 136602.

[58] B. Conings, S. Bertho, K. Vandewal, A. Senes, J. D'Haen, J. Manca, R. A. J. Janssen, *Appl. Phys. Lett.* **2010**, *96*, 163301.

[59] M. A. Ruderer, S. Guo, R. Meier, H.-Y. Chiang, V. Körstgens, J. Wiedersich, J. Perlich, S. V. Roth, P. Müller-Buschbaum, *Adv. Funct. Mater.* **2011**, *21*, 3382.

[60] R. Chintala, J. G. Tait, P. Eyben, E. Voroshazi, S. Surana, C. Fleischmann, T. Conard, W. Vandervorst, *Nanoscale* **2016**, *8*, 3629.
[61] Y. He, Y. Li, *Phys. Chem. Chem. Phys.* **2011**, *13*, 1970.
[62] S. Leach, M. Vervloet, A. Desprès, E. Bréheret, J. P. Hare, T. John Dennis, H. W. Kroto, R. Taylor, D. R. M. Walton, *Chem. Phys.* **1992**, *160*, 451.
[63] Q. Xie, E. Perez-Cordero, L. Echegoyen, *J. Am. Chem. Soc.* **1992**, *114*, 3978.
[64] D. M. Guldi, *Chem. Commun.* **2000**, 321.
[65] R. S. Ruoff, D. S. Tse, R. Malhotra, D. C. Lorents, *J. Phys. Chem.* **1993**, *97*, 3379.
[66] J. C. Hummelen, B. W. Knight, F. LePeq, F. Wudl, J. Yao, C. L. Wilkins, *J. Org. Chem.* **1995**, *60*, 532.
[67] Y. He, H.-Y. Chen, J. Hou, Y. Li, *J. Am. Chem. Soc.* **2010**, *132*, 1377.
[68] a) N. C. Cates, R. Gysel, Z. Beiley, C. E. Miller, M. F. Toney, M. Heeney, I. McCulloch, M. D. McGehee, *Nano Lett.* **2009**, *9*, 4153; b) A. C. Mayer, M. F. Toney, S. R. Scully, J. Rivnay, C. J. Brabec, M. Scharber, M. Koppe, M. Heeney, I. McCulloch, M. D. McGehee, *Adv. Funct. Mater.* **2009**, *19*, 1173.
[69] I. M. K. Ismail, S. L. Rodgers, *Carbon* **1992**, *30*, 229.
[70] a) H. Werner, T. Schedel-Niedrig, M. Wohlers, D. Herein, B. Herzog, R. Schlogl, M. Keil, A. M. Bradshaw, J. Kirschner, *J. Chem. Soc., Farad. Trans.* **1994**, *90*, 403; b) A. Tapponnier, I. Biaggio, P. Günter, *Appl. Phys. Lett.* **2005**, *86*, 112114.
[71] a) A. Hamed, Y. Y. Sun, Y. K. Tao, R. L. Meng, P. H. Hor, *Phys. Rev. B* **1993**, *47*, 10873; b) K. M. Creegan, J. L. Robbins, W. K. Robbins, J. M. Millar, R. D. Sherwood, P. J. Tindall, D. M. Cox, J. P. McCauley, D. R. Jones, *J. Am. Chem. Soc.* **1992**, *114*, 1103; c) G. H. Kroll, P. J. Benning, Y. Chen, T. R. Ohno, J. H. Weaver, L. P. F. Chibante, R. E. Smalley, *Chem. Phys. Lett.* **1991**, *181*, 112.
[72] a) A. M. Rao, M. Menon, K.-A. Wang, P. C. Eklund, K. R. Subbaswamy, D. S. Cornett, M. A. Duncan, I. J. Amster, *Chem. Phys. Lett.* **1994**, *224*, 106; b) A. M. Rao, P. Zhou, K.-A. Wang, G. T. Hager, J. M. Holden, Y. Wang, W.-T. Lee, X.-X. Bi, P. C. Eklund, D. S. Cornett, M. A. Duncan, I. J. Amster, *Science* **1993**, *259*, 955; c) J. Wang, J. Enevold, L. Edman, *Adv. Funct. Mater.* **2013**, *23*, 3220; d) P. C. Eklund, A. M. Rao, P. Zhou, Y. Wang, J. M. Holden, *Thin Solid Films* **1995**, *257*, 185.
[73] P. Zhou, Z.-H. Dong, A. M. Rao, P. C. Eklund, *Chem. Phys. Lett.* **1993**, *211*, 337.
[74] a) G. B. Adams, J. B. Page, O. F. Sankey, M. O'Keeffe, *Phys. Rev. B* **1994**, *50*, 17471; b) J. L. Segura, N. Martin, *Chem Soc Rev.* **2000**, *29*, 13; c) J. Knol, J. C. Hummelen, *J. Am. Chem. Soc.* **2000**, *122*, 3226.
[75] a) A. Dzwilewski, T. Wågberg, L. Edman, *J. Am. Chem. Soc.* **2009**, *131*, 4006; b) J. C. Hummelen, J. Knol, L. Sánchez, *Proc. SPIE* **2001**, *4108*, 76; c) J. Wang, C. Larsen, T. Wågberg, L. Edman, *Adv. Funct. Mater.* **2011**, *21*, 3723.
[76] a) H. Neugebauer, C. Brabec, J. C. Hummelen, N. S. Sariciftci, *Solar Energy Mater. Solar Cells* **2000**, *61*, 35; b) M. O. Reese, A. M. Nardes, B. L. Rupert, R. E. Larsen, D. C. Olson, M. T. Lloyd, S. E. Shaheen, D. S. Ginley, G. Rumbles, N. Kopidakis, *Adv. Funct. Mater.* **2010**, *20*, 3476; c) T. Tromholt, M. V. Madsen, J. E. Carle, M. Helgesen, F. C. Krebs, *J. Mater. Chem.* **2012**, *22*, 7592; d) S. Chambon, A. Rivaton, J.-L. Gardette, M. Firon, *Solar Energy Mater. Solar Cells* **2007**, *91*, 394.
[77] L. Ma, X. Wang, B. Wang, J. Chen, J. Wang, K. Huang, B. Zhang, Y. Cao, Z. Han, S. Qian, S. Yao, *Chem. Phys.* **2002**, *285*, 85.
[78] A. Tournebize, P.-O. Bussière, A. Rivaton, J.-L. Gardette, H. Medlej, R. C. Hiorns, C. Dagron-Lartigau, F. C. Krebs, K. Norrman, *Chem. Mater.* **2013**, *25*, 4522.
[79] a) J. R. Morton, F. Negri, K. F. Preston, *Acc. Chem. Res.* **1998**, *31*, 63; b) Y. Chen, K.-C. Lin, *J. Polym. Sci. Part A: Polym. Chem.* **1999**, *37*, 2969; c) J.-J. Yin, F. Lao, P. P. Fu, W. G. Wamer, Y. Zhao, P. C. Wang, Y. Qiu, B. Sun, G. Xing, J. Dong, X.-J. Liang, C. Chen, *Biomaterials* **2009**, *30*, 611.
[80] a) J. C. V. P. Moura, A. M. F. Oliveira-Campos, J. Griffiths, *Dyes Pigments* **1997**, *33*, 173; b) A. Zweig, W. A. Henderson, *J. Polym. Sci.: Polymer Chem. Ed.* **1975**, *13*, 993; c) J. Flood, K. E. Russell, J. K. S. Wan, *Macromolecules* **1973**, *6*, 669; d) B. M. Monroe, J. J. Mrowca, *J. Phys. Chem.* **1979**, *83*, 591.
[81] P. O. Bussière, B. Mailhot, A. Rivaton, M. F. Barthe, J. L. Gardette, M. Baba, *Polym. Degrad. Stabil.* **2008**, *93*, 1376.
[82] a) A. Aguirre, G. Janssen, E. Goovaerts, K. Colladet, D. Vanderzande, L. Lutsen, *Eur. Phys. J. - Appl. Phys.* **2006**, *36*, 285; b) A. Aguirre, S. C. J. Meskers, R. A. J. Janssen, H. J. Egelhaaf, *Org. Electron.* **2011**, *12*, 1657.
[83] a) R. D. Scurlock, P. R. Ogilby, *J. Phys. Chem.* **1989**, *93*, 5493; b) A. Sperlich, H. Kraus, C. Deibel, H. Blok, J. Schmidt, V. Dyakonov, *J. Phys. Chem. B* **2011**, *115*, 13513.
[84] F. Prat, R. Stackow, R. Bernstein, W. Qian, Y. Rubin, C. S. Foote, *J. Phys. Chem. A* **1999**, *103*, 7230.
[85] S. Cook, H. Ohkita, Y. Kim, J. J. Benson-Smith, D. D. C. Bradley, J. R. Durrant, *Chem. Phys. Lett.* **2007**, *445*, 276.
[86] J.-M. Zhuo, L.-H. Zhao, R.-Q. Png, L.-Y. Wong, P.-J. Chia, J.-C. Tang, S. Sivaramakrishnan, M. Zhou, E. C. W. Ou, S.-J. Chua, W.-S. Sim, L.-L. Chua, P. K. H. Ho, *Adv. Mater.* **2009**, *21*, 4747.
[87] V. Dyakonov, E. Frankevich, *Chem. Phys.* **1998**, *227*, 203.
[88] J. Peet, J. Y. Kim, N. E. Coates, W. L. Ma, D. Moses, A. J. Heeger, G. C. Bazan, *Nat. Mater.* **2007**, *6*, 497.
[89] D. Di Nuzzo, A. Aguirre, M. Shahid, V. S. Gevaerts, S. C. J. Meskers, R. A. J. Janssen, *Adv. Mater.* **2010**, *22*, 4321.
[90] G. Grancini, M. De Bastiani, N. Martino, D. Fazzi, H. J. Egelhaaf, T. Sauermann, M. R. Antognazza, G. Lanzani, M. Caironi, L. Franco, A. Petrozza, *Physical Chem. Chem. Phys.* **2014**, *16*, 8294.
[91] a) Z. Li, H. C. Wong, Z. Huang, H. Zhong, C. H. Tan, W. C. Tsoi, J. S. Kim, J. R. Durrant, J. T. Cabral, *Nat. Commun.* **2013**, *4*, 2227; b) I. Cardinaletti, J. Kesters, S. Bertho, B. Conings, F. Piersimoni, J. D'Haen, L. Lutsen, M. Nesladek, B. Van Mele, G. Van Assche, K. Vandewal, A. Salleo, D. Vanderzande, W. Maes, J. V. Manca, *J. Photonics Energy* **2014**, *4*, 040997; c) F. Piersimoni, G. Degutis, S. Bertho, K. Vandewal, D. Spoltore, T. Vangerven, J. Drijkoningen, M. K. Van Bael, A. Hardy, J. D'Haen, W. Maes, D. Vanderzande, M. Nesladek, J. Manca, *J. Polym. Sci. B: Polym. Phys.* **2013**, *51*, 1209; d) H. C. Wong, A. M. Higgins, A. R. Wildes, J. F. Douglas, J. T. Cabral, *Adv. Mater.* **2013**, *25*, 985; e) H. C. Wong, Z. Li, C. H. Tan, H. Zhong, Z. Huang, H. Bronstein, I. McCulloch, J. T. Cabral, J. R. Durrant, *ACS Nano* **2014**, *8*, 1297.
[92] Q. Burlingame, X. Tong, J. Hankett, M. Slootsky, Z. Chen, S. R. Forrest, *Energy Environ. Sci.* **2015**, *8*, 1005.
[93] V. Ramamurthy, K. Venkatesan, *Chem. Rev.* **1987**, *87*, 433.
[94] S. T. Turner, P. Pingel, R. Steyrleuthner, E. J. W. Crossland, S. Ludwigs, D. Neher, *Adv. Funct. Mater.* **2011**, *21*, 4640.
[95] M. C. Scharber, M. Koppe, J. Gao, F. Cordella, M. A. Loi, P. Denk, M. Morana, H.-J. Egelhaaf, K. Forberich, G. Dennler, R. Gaudiana, D. Waller, Z. Zhu, X. Shi, C. J. Brabec, *Adv. Mater.* **2010**, *22*, 367.
[96] Y. Wang, J. M. Holden, Z.-H. Dong, X.-X. Bi, P. C. Eklund, *Chem. Phys. Lett.* **1993**, *211*, 341.
[97] M. Suzuki, T. Iida, K. Nasu, *Phys. Rev. B* **2000**, *61*, 2188.
[98] J. W. Arbogast, A. P. Darmanyan, C. S. Foote, F. N. Diederich, R. L. Whetten, Y. Rubin, M. M. Alvarez, S. J. Anz, *J. Phys. Chem.* **1991**, *95*, 11.
[99] a) D. M. Guldi, M. Prato, *Acc. Chem. Res.* **2000**, *33*, 695; b) A. Nakamura, M. Ichida, T. Yajima, H. Shinohara, Y. Saitoh, *J. Lumin.* **1995**, *66–67*, 383.
[100] E. F. Sheka, *Chem. Phys. Lett.* **2007**, *438*, 119.

[101] a) H. Hoppe, N. S. Sariciftci, *J. Mater. Chem.* **2006**, *16*, 45; b) J. Nelson, *Mater. Today* **2011**, *14*, 462; c) I. Etxebarria, J. Ajuria, R. Pacios, *Org. Electron.* **2015**, *19*, 34.

[102] a) E. Klimov, W. Li, X. Yang, G. G. Hoffmann, J. Loos, *Macromolecules* **2006**, *39*, 4493; b) A. Swinnen, I. Haeldermans, M. vande Ven, J. D'Haen, G. Vanhoyland, S. Aresu, M. D'Olieslaeger, J. Manca, *Adv. Funct. Mater.* **2006**, *16*, 760.

[103] a) L. Derue, C. Lecourtier, T. Gorisse, L. Hirsch, O. Dautel, G. Wantz, *RSC Adv.* **2015**, *5*, 3840; b) F. Goubard, G. Wantz, *Polym. Int.* **2014**, *63*, 1362.

[104] Y. Wang, J. M. Holden, X.-X. Bi, P. C. Eklund, *Chem. Phys. Lett.* **1994**, *217*, 413.

[105] B. C. Schroeder, Z. Li, M. A. Brady, G. C. Faria, R. S. Ashraf, C. J. Takacs, J. S. Cowart, D. T. Duong, K. H. Chiu, C.-H. Tan, J. T. Cabral, A. Salleo, M. L. Chabinyc, J. R. Durrant, I. McCulloch, *Angew. Chem. Int. Ed.* **2014**, *53*, 12870.

[106] a) Y. Zhang, H.-L. Yip, O. Acton, S. K. Hau, F. Huang, A. K. Y. Jen, *Chem. Mater.* **2009**, *21*, 2598; b) S.-O. Kim, D. Sung Chung, H. Cha, J. Wan Jang, Y.-H. Kim, J.-W. Kang, Y.-S. Jeong, C. E. Park, S.-K. Kwon, *Solar Energy Mater. Solar Cells* **2011**, *95*, 432.

[107] a) G. Wantz, L. Derue, O. Dautel, A. Rivaton, P. Hudhomme, C. Dagron-Lartigau, *Polym. Int.* **2014**, *63*, 1346; b) J. W. Rumer, I. McCulloch, *Mater. Today* **2015**, *18*, 425.

[108] a) C.-Y. Nam, Y. Qin, Y. S. Park, H. Hlaing, X. Lu, B. M. Ocko, C. T. Black, R. B. Grubbs, *Macromolecules* **2012**, *45*, 2338; b) B. Gholamkhass, S. Holdcroft, *Chem. Mater.* **2010**, *22*, 5371.

[109] L. Derue, O. Dautel, A. Tournebize, M. Drees, H. Pan, S. Berthumeyrie, B. Pavageau, E. Cloutet, S. Chambon, L. Hirsch, A. Rivaton, P. Hudhomme, A. Facchetti, G. Wantz, *Adv. Mater.* **2014**, *26*, 5831.

[110] a) Y.-J. Cheng, C.-H. Hsieh, P.-J. Li, C.-S. Hsu, *Adv. Funct. Mater.* **2011**, *21*, 1723; b) M. Drees, H. Hoppe, C. Winder, H. Neugebauer, N. S. Sariciftci, W. Schwinger, F. Schaffler, C. Topf, M. C. Scharber, Z. Zhu, R. Gaudiana, *J. Mater. Chem.* **2005**, *15*, 5158.

[111] a) H. H. Ramanitra, H. Santos Silva, B. A. Bregadiolli, A. Khoukh, C. M. S. Combe, S. A. Dowland, D. Bégué, C. F. O. Graeff, C. Dagron-Lartigau, A. Distler, G. Morse, R. C. Hiorns, *Macromolecules* **2016**, *49*, 1681; b) M. Hufnagel, M. Thelakkat, *J. Polym. Sci. Part B: Polym. Phys.* **2016**, *54*, 1125; c) M. Stephen, H. H. Ramanitra, H. Santos Silva, S. Dowland, D. Begue, K. Genevicius, K. Arlauskas, G. Juska, G. E. Morse, A. Distler, R. C. Hiorns, *Chem. Commun.* **2016**, *52*, 6107; d) A. Cravino, G. Zerza, M. Maggini, S. Bucella, M. Svensson, M. R. Andersson, H. Neugebauer, N. S. Sariciftci, *Chem. Commun.* **2000**, 2487; e) A. M. Ramos, M. T. Rispens, J. K. J. van Duren, J. C. Hummelen, R. A. J. Janssen, *J. Am. Chem. Soc.* **2001**, *123*, 6714; f) N. G. Martin, *Francesco, Fullerene Polym.*, Wiley-VCH, Weinheim, **2009**, p; g) M. Gutierrez Nava, S. Setayesh, A. Rameau, P. Masson, J.-F. Nierengarten, *New J. Chem.* **2002**, *26*, 1584; h) S. Miyanishi, Y. Zhang, K. Tajima, K. Hashimoto, *Chem. Commun.* **2010**, *46*, 6723; i) P. D. Topham, A. J. Parnell, R. C. Hiorns, *J. Polym. Sci. Part B: Polym. Phys.* **2011**, *49*, 1131.

[112] Y.-W. Su, S.-C. Lan, K.-H. Wei, *Mater. Today* **2012**, *15*, 554.

[113] K. Sivula, Z. T. Ball, N. Watanabe, J. M. J. Fréchet, *Adv. Mater.* **2006**, *18*, 206.

[114] a) C.-Y. Chen, C.-S. Tsao, Y.-C. Huang, H.-W. Liu, W.-Y. Chiu, C.-M. Chuang, U. S. Jeng, C.-J. Su, W.-R. Wu, W.-F. Su, L. Wang, *Nanoscale* **2013**, *5*, 7629; b) C. Lindqvist, J. Bergqvist, O. Bäcke, S. Gustafsson, E. Wang, E. Olsson, O. Inganäs, M. R. Andersson, C. Müller, *Appl. Phys. Lett.* **2014**, *104*, 153301; c) H.-W. Liu, D.-Y. Chang, W.-Y. Chiu, S.-P. Rwei, L. Wang, *J. Mater. Chem.* **2012**, *22*, 15586; d) J. J. Richards, A. H. Rice, R. D. Nelson, F. S. Kim, S. A. Jenekhe, C. K. Luscombe, D. C. Pozzo, *Adv. Funct. Mater.* **2013**, *23*, 514; e) Y. Santo, I. Jeon, K. Sheng Yeo, T. Nakagawa, Y. Matsuo, *Appl. Phys. Lett.* **2013**, *103*, 073306; f) P. Cheng, C. Yan, Y. Wu, J. Wang, M. Qin, Q. An, J. Cao, L. Huo, F. Zhang, L. Ding, Y. Sun, W. Ma, X. Zhan, *Adv. Mater.* **2016**, DOI: 10.1002/adma.201602067; g) N. A. Cooling, E. F. Barnes, F. Almyahi, K. Feron, M. F. Al-Mudhaffer, A. Al-Ahmad, B. Vaughan, T. R. Andersen, M. J. Griffith, A. S. Hart, A. G. Lyons, W. J. Belcher, P. C. Dastoor, *J. Mater. Chem. A* **2016**, *4*, 10274.

[115] L. M. Andersson, Y.-T. Hsu, K. Vandewal, A. B. Sieval, M. R. Andersson, O. Inganäs, *Org. Electron.* **2012**, *13*, 2856.

[116] a) S. Cataldo, P. Salice, E. Menna, B. Pignataro, *Energy Environ. Sci.* **2012**, *5*, 5919; b) A. J. Ferguson, J. L. Blackburn, N. Kopidakis, *Mater. Lett.* **2013**, *90*, 115; c) G. Keru, P. G. Ndungu, V. O. Nyamori, *Int. J. Energy Res.* **2014**, *38*, 1635; d) M. S. Arnold, J. L. Blackburn, J. J. Crochet, S. K. Doorn, J. G. Duque, A. Mohite, H. Telg, *Phys. Chem. Chem. Phys.* **2013**, *15*, 14896.

[117] R. B. Weisman, S. M. Bachilo, *Nano Lett.* **2003**, *3*, 1235.

[118] a) J. M. Lee, J. S. Park, S. H. Lee, H. Kim, S. Yoo, S. O. Kim, *Adv. Mater.* **2011**, *23*, 629; b) D. Jana, C.-L. Sun, L.-C. Chen, K.-H. Chen, *Prog. Mater. Sci.* **2013**, *58*, 565.

[119] J. J. Crochet, S. Hoseinkhani, L. Lüer, T. Hertel, S. K. Doorn, G. Lanzani, *Phys. Rev. Lett.* **2011**, *107*, 257402.

[120] J. N. Coleman, U. Khan, W. J. Blau, Y. K. Gun'ko, *Carbon* **2006**, *44*, 1624.

[121] S. Iijima, C. Brabec, A. Maiti, J. Bernholc, *J. Chem. Phys.* **1996**, *104*, 2089.

[122] T. Lin, V. Bajpai, T. Ji, L. Dai, *Aus. J. Chem.* **2003**, *56*, 635.

[123] P. C. P. Watts, P. K. Fearon, W. K. Hsu, N. C. Billingham, H. W. Kroto, D. R. M. Walton, *J. Mater. Chem.* **2003**, *13*, 491.

[124] a) C.-Y. Chen, C. T. Jafvert, *Carbon* **2011**, *49*, 5099; b) B. Wu, D. Zhu, S. Zhang, W. Lin, G. Wu, B. Pan, *J. Colloid Interface Sci.* **2015**, *439*, 98; c) C.-Y. Chen, C. T. Jafvert, *Environ. Sci. Technol.* **2010**, *44*, 6674; d) Y. S. Hwang, X. Qu, Q. Li, *Carbon* **2013**, *55*, 81; e) I. Fenoglio, M. Tomatis, D. Lison, J. Muller, A. Fonseca, J. B. Nagy, B. Fubini, *Free Radical Biol. Med.* **2006**, *40*, 1227; f) X. Qu, P. J. J. Alvarez, Q. Li, *Environ. Sci. Technol.* **2013**, *47*, 14080.

[125] a) S. Morlat-Therias, E. Fanton, J.-L. Gardette, S. Peeterbroeck, M. Alexandre, P. Dubois, *Polym. Degrad. Stabil.* **2007**, *92*, 1873; b) N. T. Dintcheva, F. P. La Mantia, V. Malatesta, *Polym. Degrad. Stabil.* **2009**, *94*, 162; c) N. T. Dintcheva, R. Arrigo, F. Catalanotto, E. Morici, *Polym. Degrad. Stabil.* **2015**, *118*, 24; d) P.-O. Bussière, J. Peyroux, G. Chadeyron, S. Therias, *Polym. Degrad. Stabil.* **2013**, *98*, 2411.

[126] a) R. C. Tenent, T. M. Barnes, J. D. Bergeson, A. J. Ferguson, B. To, L. M. Gedvilas, M. J. Heben, J. L. Blackburn, *Adv. Mater.* **2009**, *21*, 3210; b) M.-H. Ham, G. L. C. Paulus, C. Y. Lee, C. Song, K. Kalantar-zadeh, W. Choi, J.-H. Han, M. S. Strano, *ACS Nano* **2010**, *4*, 6251; c) J. M. Holt, A. J. Ferguson, N. Kopidakis, B. A. Larsen, J. Bult, G. Rumbles, J. L. Blackburn, *Nano Lett.* **2010**, *10*, 4627; d) F. Schöppler, C. Mann, T. C. Hain, F. M. Neubauer, G. Privitera, F. Bonaccorso, D. Chu, A. C. Ferrari, T. Hertel, *J. Phys. Chem. C* **2011**, *115*, 14682; e) D. J. Bindl, N. S. Safron, M. S. Arnold, *ACS Nano* **2010**, *4*, 5657.

[127] M. W. Rowell, M. A. Topinka, M. D. McGehee, H.-J. Prall, G. Dennler, N. S. Sariciftci, L. Hu, G. Gruner, *Appl. Phys. Lett.* **2006**, *88*, 233506.

[128] K. T. Dembele, R. Nechache, L. Nikolova, A. Vomiero, C. Santato, S. Licoccia, F. Rosei, *J. Power Sources* **2013**, *233*, 93.

[129] P. J. Goutam, D. K. Singh, P. K. Giri, P. K. Iyer, *J. Phys. Chem. B* **2011**, *115*, 919.

[130] a) R. Ratha, P. J. Goutam, P. K. Iyer, *Org. Electron.* **2014**, *15*, 1650; b) V. Singh, S. Arora, M. Arora, V. Sharma, R. P. Tandon, *Phys. Lett. A* **2014**, *378*, 3046.

[131] M. S. Arnold, S. I. Stupp, M. C. Hersam, *Nano Lett.* **2005**, *5*, 713.